Simulation of Third Generation CDMA Systems

by

Fakhrul Alam

Thesis submitted to the faculty of the
Virginia Polytechnic Institute & State University
in partial fulfillment of the requirements of the degree

MASTER OF SCIENCE

in

Electrical Engineering

Approved:

_____

Dr. Brian D. Woerner, Chairman

_____ _____

Dr. W. H. Tranter Dr. Jeffrey H. Reed

December 15, 1999

Blacksburg, Virginia

Keywords: Wideband CDMA, Third Generation CDMA Systems, Wireless Communications, Simulation

Simulation of Third Generation CDMA Systems

Fakhrul Alam

ABSTRACT

The goal for the next generation of mobile communications system is to seamlessly integrate a wide variety of communication services such as high speed data, video and multimedia traffic as well as voice signals. The technology needed to tackle the challenges to make these services available is popularly known as the Third Generation (3G) Cellular Systems. One of the most promising approaches to 3G is to combine a Wideband Code Division Multiple Access (WCDMA) air interface with the fixed network of Global System for Mobile communications (GSM). In this thesis a signal simulator was implemented according to the physical layer specification of the IMT-2000 WCDMA system. The data is transmitted in a frame by frame basis through a time varying channel. The transmitted signal is corrupted by multiple access interference which is generated in a structured way rather than treating it as Additive White Gaussian Noise (AWGN). The signal is further corrupted by AWGN at the front end of the receiver. Simple rake diversity combining is employed at the receiver. We investigate the bit error rate at both uplink and downlink for different channel conditions. Performance improvement due to error correction coding scheme is shown. The simulator developed can be an invaluable tool for investigating the design and implementation of WCDMA systems.

Acknowledgments

I would like to express my gratitude to Dr. Brian D. Woerner for his constant encouragement and belief in me. He has been everything that one could want in an advisor. I am deeply indebted to my committee members Dr. Jeffrey H. Reed and Dr. W. H. Tranter who have been extremely helpful both inside and outside the class. I also want to thank LGIC for sponsoring this research work. Special thanks to Raqibul Mostafa for introducing me to WCDMA and his invaluable insights. Yufei Wu deserves my thanks for going through the codes and providing with corrections and comments. I appreciate the help of Pulakesh Roy and James Hicks during the implementation of the simulator. Thanks to Parvez Ahmad, Masudur Rahman Kazi Zahid and Sujan E. Bin Wadud for reviewing my thesis and providing valuable feedback. I thank Rennie Givens for all the administrative work. Finally, most of all, I thank my parents for their unconditional love and support.

Contents

List of Tables

List of Figures

Chapter 1

Introduction

The goal for the next generation of mobile communications system is to seamlessly provide a wide variety of communication services to anybody, anywhere, anytime. The intended service for next generation mobile phone users include services like transmitting high speed data, video and multimedia traffic as well as voice signals. The technology needed to tackle the challenges to make these services available is popularly known as the Third Generation (3G) Cellular Systems. The first generation systems are represented by the analog mobile systems designed to carry the voice application traffic. Their subsequent digital counterparts are known as second generation cellular systems. Third generation systems mark a significant leap, both in applications and capacity, from the current second generation standards. Whereas the current digital mobile phone systems are optimized for voice communications, 3G communicators are oriented towards multimedia message capability.

1.1 First Generation Cellular Systems

The first generation cellular systems generally employ analog Frequency Modulation (FM) techniques. The Advanced Mobile Phone System (AMPS) is the most notable of the

first generation systems. AMPS was developed by the Bell Telephone System. It uses FM technology for voice transmission and digital signaling for control information. Other first generation systems include:

- Narrowband AMPS (NAMPS)
- Total Access Cellular System (TACS)
- Nordic Mobile Telephone System (NMT-900)

All the first generation cellular systems employ Frequency Division Multiple Access (FDMA) with each channel assigned to a unique frequency band within a cluster of cells.

1.2 Second Generation Cellular Systems

The rapid growth in the number of subscribers and the proliferation of many incompatible first generation systems were the main reason behind the evolution towards second generation cellular systems. Second generation systems take the advantage of compression and coding techniques associated with digital technology. All the second generation systems employ digital modulation schemes. Multiple access techniques like Time Division Multiple Access (TDMA) and Code Division Multiple Access (CDMA) are used along with FDMA in the second generation systems. Second generation cellular systems include:

- United States Digital Cellular (USDC) standards IS-54 and IS-136
- Global System for Mobile communications (GSM)
- Pacific Digital Cellular (PDC)
- cdmaOne

1.3 Third Generation Cellular Systems

Third generation cellular systems are being designed to support wideband services like high speed Internet access, video and high quality image transmission with the same quality as the fixed networks. The primary requirements of the next generation cellular systems are [1]:

- Voice quality comparable to Public Switched Telephone Network (PSTN).
- Support of high data rate. The following table shows the data rate requirement of the 3G systems

Table 1.1: 3G Data Rate Requirements

Mobility Needs	Minimum Data Rate
Vehicular	144 kbps
Outdoor to indoor and pedestrian	384 kbps
Indoor Office	2 Mbps

- Support of both packet-switched and circuit-switched data services.
- More efficient usage of the available radio spectrum
- Support of a wide variety of mobile equipment
- Backward Compatibility with pre-existing networks and flexible introduction of new services and technology
- An adaptive radio interface suited to the highly asymmetric nature of most Internet communications: a much greater bandwidth for the downlink than the uplink.

Research efforts have been underway for more than a decade to introduce multimedia capabilities into mobile communications. Different standard agencies and governing bodies are trying to integrate a wide variety of proposals for third generation cellular systems. The following figure, adopted from [1], shows the evolution of third generation cellular systems:

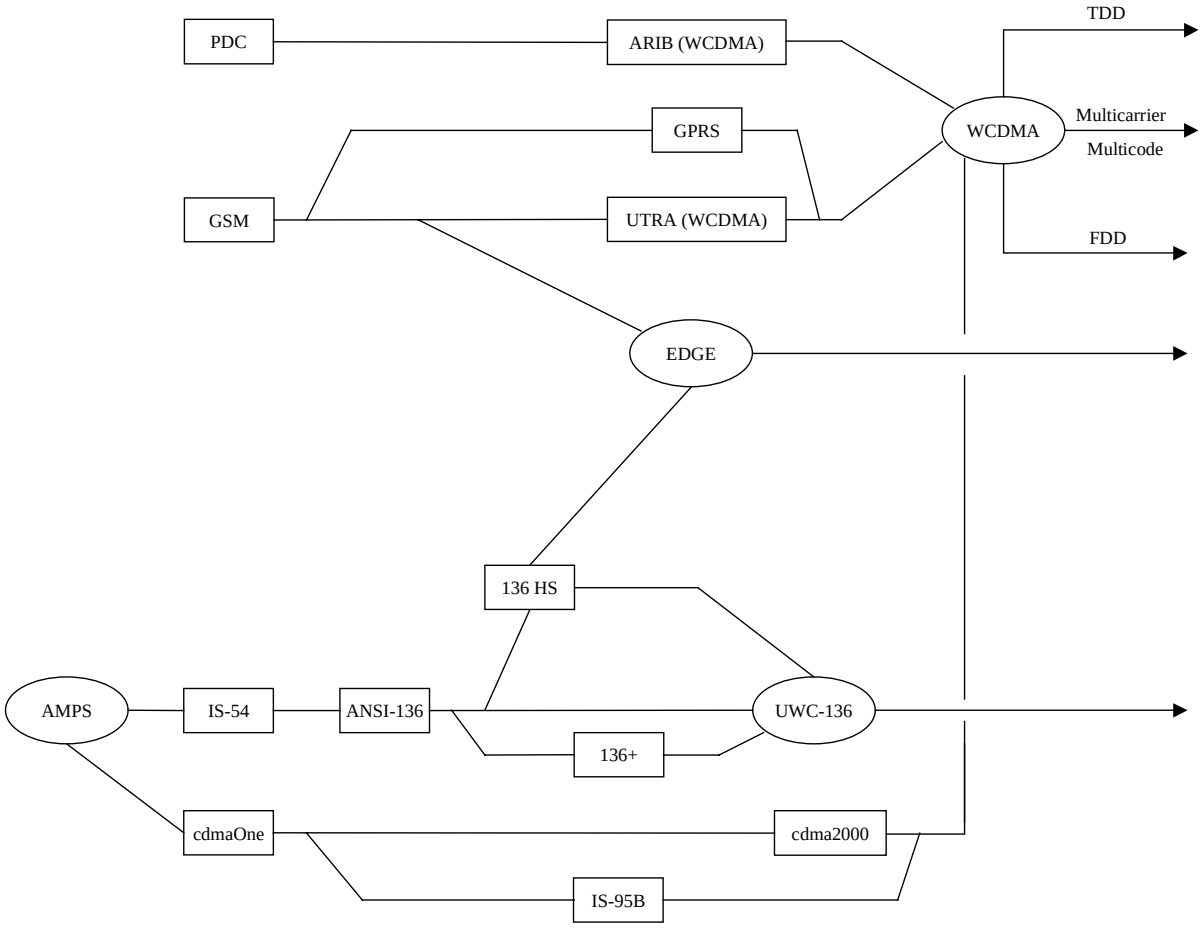

Figure 1.1: Evolution of 3G

References [2] and [3] provide further discussion on the evolution of third generation cellular systems.

1.4. WCDMA: Air Interface for 3G

One of the most promising approaches to 3G is to combine a Wideband CDMA (WCDMA) air interface with the fixed network of GSM. Several proposal supporting WCDMA were submitted to the International Telecommunication Union (ITU) and its International Mobile Telecommunications for the year 2000 (IMT2000) initiative for 3G. Among several organizations trying to merge their various WCDMA proposals are

- Japan's Association of Radio Industry and Business (ARIB)
- Alliance for Telecommunications Industry Solutions (ATIS)
- T1P1
- European Telecommunications Standards Institute (ETSI) through its Special Mobile Group (SMG)

All these schemes try to take advantage of the WCDMA radio techniques without ignoring the numerous advantages of the already existing GSM networks. The standard that has emerged is based on ETSI's Universal Mobile Telecommunication System (UMTS) and is commonly known as UMTS Terrestrial Radio Access (UTRA) [1]. The access scheme for UTRA is Direct Sequence Code Division Multiple Access (DS-CDMA). The information is spread over a band of approximately 5 MHz. This wide bandwidth has given rise to the name *Wideband* CDMA or WCDMA. There are two different modes namely

- Frequency Division Duplex (FDD)
- Time Division Duplex (TDD)

Since different regions have different frequency allocation schemes, the capability to operate in either FDD or TDD mode allows for efficient utilization of the available spectrum. A brief definition of FDD and TDD modes is given next.

FDD: The uplink and downlink transmissions employ two separated frequency bands for this duplex method. A pair of frequency bands with specified separation is assigned for a connection.

TDD: In this duplex method**,** uplink and downlink transmissions are carried over the same frequency band by using synchronized time intervals Thus time slots in a physical channel are divided into transmission and reception part.

We developed the simulator for a WCDMA system operating in the FDD mode. So all the system description provided in chapter 2 holds for the FDD mode only.

1.4.1 WCDMA Key Features

The key operational features of the WCDMA radio interface are listed below [3], [4]:

- Support of high data rate transmission: 384 kbps with wide area coverage, 2 Mbps with local coverage.
- High service flexibility: support of multiple parallel variable rate services on each connection.
- Both Frequency Division Duplex (FDD) and Time Division Duplex (TDD).
- Built in support for future capacity and coverage enhancing technologies like adaptive antennas, advanced receiver structures and transmitter diversity.
- Support of inter frequency hand over and hand over to other systems, including hand over to GSM.
- Efficient packet access.

1.4.2 WCDMA Key Technical Characteristics

The following table shows the key technical features of the WCDMA radio interface:

Table 1.2: WCDMA Key Technical Characteristics

Multiple Access Scheme	DS-CDMA
Duplex Scheme	FDD/TDD
Packet Access	Dual mode (Combined and dedicated channel)
Multirate/Variable rate scheme	Variable spreading factor and multi-code
Chip Rate	3.84 Mcps
Carrier Spacing	4.4-5.2 MHz (200 kHz carrier raster)
Frame Length	10 ms
Inter Base Station synchronization	FDD: No accurate synchronization needed TDD: Synchronization required
Channel Coding Scheme	Convolutional Code (rate 1/2 and 1/3) Turbo code

The chip rate may be extended to two or three times the standard 3.84 Mcps to accommodate for data rates higher than 2 Mbps. The 200 kHz carrier raster has been chosen to facilitate coexistence and interoperability with GSM.

1.5 Outline of Thesis

A brief description of key features of WCDMA system is provided in Chapter one. The physical layer of the WCDMA system is described in detail in Chapter two. Chapter three describes the WCDMA simulator. BER simulation results for WCDMA system

employing rake reception in different multipath environment is shown in Chapter four. Chapter four also shows a test case of error correction coding applied to an uplink voice service application of 9.6 kbps. Chapter five concludes the thesis along with providing some future research directions.

Chapter 2

WCDMA Physical Layer

This chapter provides a layer 1 (also termed as physical layer) description of the radio access network of a WCDMA system operating in the FDD mode. The spreading and modulation operation for the Dedicated Physical Channels (DPCH) at both the links is illustrated in detail since it is the most essential part of the simulator that we implemented. The uplink and downlink data structure for the DPCHs is described. The spreading and scrambling codes used in both the links are investigated. The spreading modulation and data structure for Physical Random Access channel (PRACH), Synchronization Channel (SCH), etc. are described in detail in [5] and [6] along with those of the DPDCHs.

2.1 Physical Channel Structure

WCDMA defines two dedicated physical channels in both links:

- Dedicated Physical Data Channel (DPDCH): to carry dedicated data generated at layer 2 and above.
- Dedicated Physical Control Channel (DPCCH): to carry layer 1 control information.

Each connection is allocated one DPCCH and zero, one or several DPDCHs. In addition, there are common physical channels defined as:

- Primary and secondary Common Control Physical Channels (CCPCH) to carry downlink common channels
- Synchronization Channels (SCH) for cell search
- Physical Random Access Channel (PRACH)

The spreading and modulation for the DPDCH and the DPCCH for both the links are described in the following two subsections.

2.1.1 Uplink Spreading and Modulation

In the uplink the data modulation of both the DPDCH and the DPCCH is Binary Phase Shift Keying (BPSK). The modulated DPCCH is mapped to the Q-channel, while the first DPDCH is mapped to the I-channel. Subsequently added DPDCHs are mapped alternatively to the I or the Q-channel. Spreading Modulation is applied after data modulation and before pulse shaping. The spreading modulation used in the uplink is dual channel QPSK. Spreading modulation consists of two different operations. The first one is spreading where each data symbol is spread to a number of chips given by the spreading factor. This increases the bandwidth of the signal. The second operation is scrambling where a complex valued scrambling code is applied to spread signal. Figure 2.1 shows the spreading and modulation for an uplink user. The uplink user has a DPDCH and a DPCCH.

The bipolar data symbols on I and Q branches are independently multiplied by different channelization codes. The channelization codes are known as Orthogonal Variable Spreading Factor (OVSF) codes. OVSF codes are discussed in section 2.4.

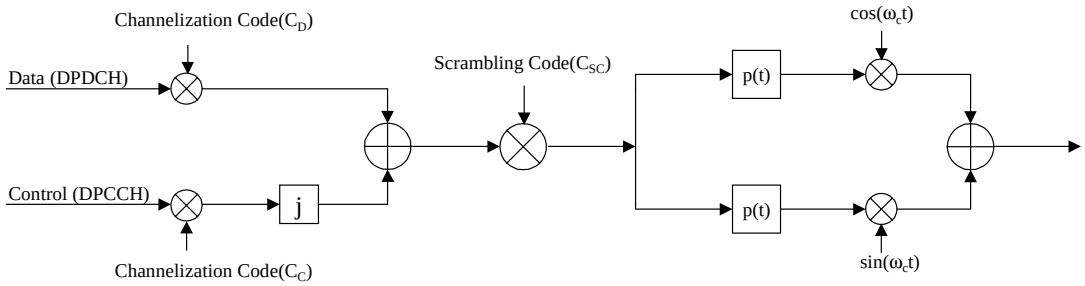

Figure 2.1: Uplink Spreading and Modulation

The resultant signal is multiplied by a complex scrambling code. The complex scrambling code is a unique signature of the mobile station. Next, the scrambled signal is pulse shaped. Square-Root Raised Cosine filters with roll-off factor of 0.22 are employed for pulse shaping. The pulse shaped signal is subsequently upconverted as shown in Figure 2.1.

The application of a complex scrambling code with spreading modulation as described above is usually termed as Hybrid Phase Shift Keying (HPSK). HPSK reduces the peak-to-average power of the mobile station by generating the complex scrambling sequence in a special way [7]. The generation of complex scrambling code is discussed in section 2.5.

The spreading factor for the control channel is always set at the highest value which is 256. This improves the noise immunity at the control channel by taking advantage of the highest possible processing gain.

2.1.2 Downlink Spreading and Modulation

Quaternary Phase Shift Keying (QPSK) is applied for data modulation in the downlink. Each pair of two bits are serial-to-parallel converted and mapped to the I and Q branches respectively. The data in the I and Q branches are spread to the chip rate by the same channelization code. The channelization code is the same OVSF codes mentioned in section 2.1.1. This spread signal is then scrambled by a cell specific scrambling code. Figure

2.2 shows the spreading and modulation for a downlink user. The downlink user has a DPDCH and a DPCCH. Additional DPDCHs are QPSK modulated and spread with different channelization codes.

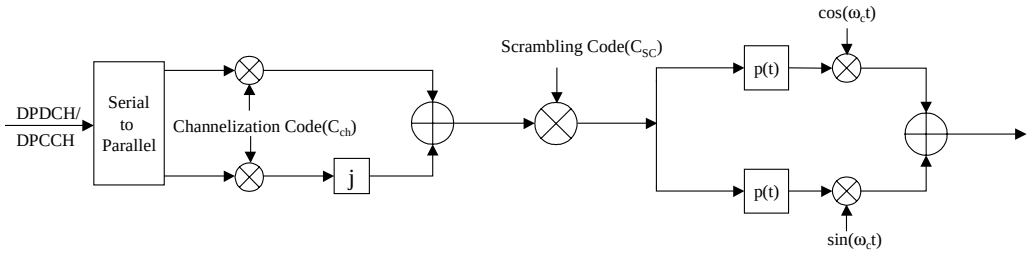

Figure 2.2: Downlink Spreading and Modulation

We can observe some differences between the spreading and modulation in the downlink and that in the uplink. The data modulation is QPSK in downlink whereas it is BPSK for the uplink. The data rates in the I and Q-channels are the same in the downlink whereas data rates in the I and Q-channel of the uplink may be different. The scrambling code is cell specific in the downlink, whereas it is mobile station specific in the uplink.

As in the uplink, Square-Root Raised Cosine filters with roll-off factor of 0.22 are employed for pulse shaping. The pulse shaped signal is subsequently upconverted as shown in Figure 2.2. The OVSF codes and the scrambling codes are described in sections 2.4 and 2.5 respectively.

2.2 Uplink Frame Structure

Figure 2.3 shows the principal frame structure of the uplink dedicated physical channels. Each frame of 10 ms is split into 15 slots. Each slot is of length 2560 chips, corresponding to one power control period. The super frame length is 720 ms; i.e. a super frame corresponds to 72 frames.

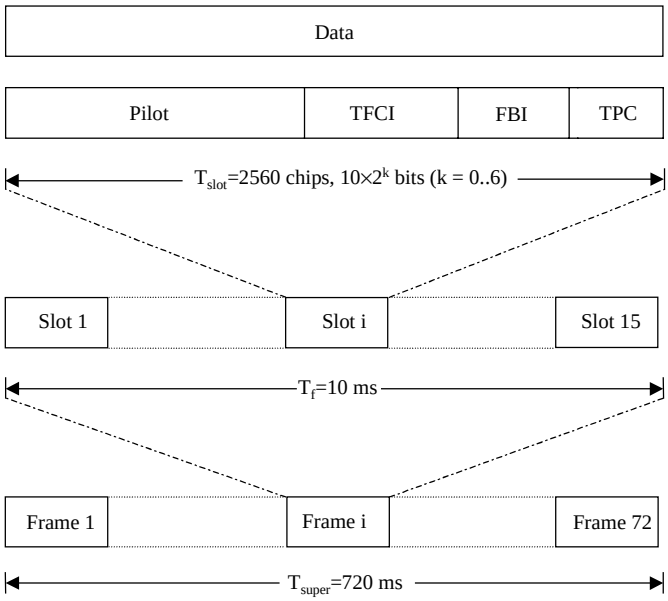

Figure 2.3: Frame Structure for Uplink DPDCH/DPCCH

Pilot bits assist coherent demodulation and channel estimation. TFCI stands for transport format combination indicator and is used to indicate and identify several simultaneous services. Feedback Information (FBI) bits are to be used to support techniques requiring feedback. TPC which stands for transmit power control is used for power control purposes. The exact number of bits of these different uplink DPCCH fields is given in [6].

The parameter k in Figure 2.3 determines the number of bits in each slot. It is related to spreading factor (SF) of the physical channel as

$$SF = \frac{256}{2^k} \qquad \textbf{(2.1)}$$

The spreading factor thus may range from 256 down to 4. The spreading factor is selected according to the data rate.

2.3 Downlink Frame Structure

Figure 2.4 shows the principal frame structure of the downlink dedicated physical channels. As in the uplink, each frame of 10 ms is split into 15 slots. Each slot is of length 2560 chips, corresponding to one power control period. A super frame corresponds to 720 ms, i.e. the super frame length corresponds to 72 frames.

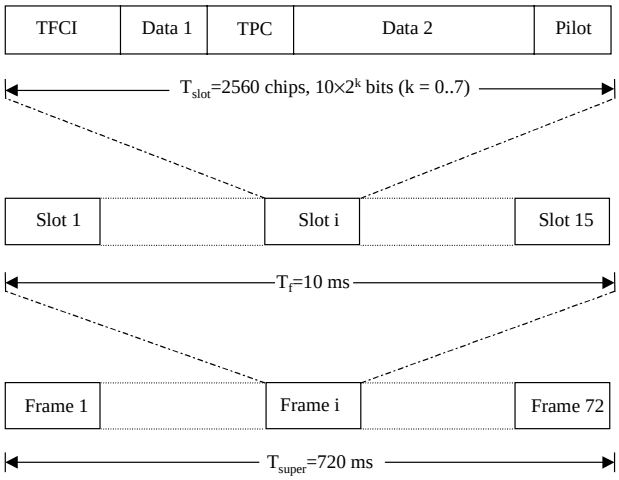

Figure 2.4: Frame Structure for Downlink DPCH

The parameter k is related to the SF of the physical channel as

$$SF = \frac{512}{2^k} \qquad \textbf{(2.2)}$$

The spreading factor thus has a range of 4 to 512. Thus an additional spreading factor of 512 is permitted at the downlink. The different control bits have similar meaning to those in the uplink. The exact number of bits in each of the downlink DPCH fields is described in [6].

2.4 Uplink Spreading Codes

The spreading code, as the name suggests, spreads the data to the chip rate of 3.84 mega chips per second (Mcps). The most important purpose of the spreading codes is to help preserve orthogonality among different physical channels of the uplink user. As mentioned in section 2.1.1, OVSF codes are employed as uplink spreading codes. OVSF codes can be explained using the code tree shown in the next figure. The subscript here gives the spreading factor and the argument within the parenthesis provides the code number for that particular spreading factor.

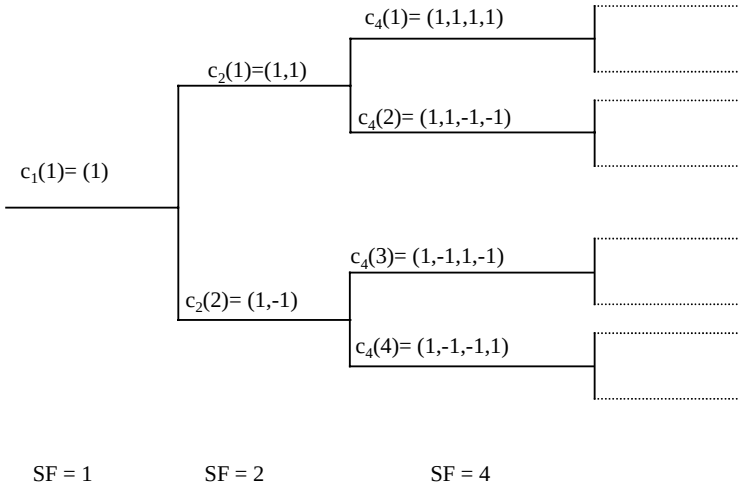

Figure 2.5: Code-tree for Generation of OVSF Codes

Each level in the code tree defines spreading codes of length SF, corresponding to a particular spreading factor of SF. The number of codes for a particular spreading factor is equal to the spreading factor itself. All the codes of the same level constitute a set and they are orthogonal to each other. Any two codes of different levels are orthogonal to each other as long as one of them is not the mother of the other code [8]. For example the codes $c_{16}(2)$,$c_8(1)$ and $c_4(1)$ are all mother codes of $c_{32}(3)$ and hence are not orthogonal to $c_{32}(32)$. Thus all the codes within the code tree can not be used simultaneously by a mobile station. A

code can be used by an MS if and only if no other code on the path from the specific code to the root of the tree or in the sub-tree below the specific code is used by the same MS [5]. The generation method of OVSF can be explained with the help of the following matrix equations:

$$\left[c_1(1)\right] = 1$$

$$\begin{bmatrix} c_2(1) \\ c_2(2) \end{bmatrix} = \begin{bmatrix} c_1(1) & c_1(1) \\ c_1(1) & \overline{c_1(1)} \end{bmatrix} = \begin{bmatrix} 1 & 1 \\ 1 & -1 \end{bmatrix}$$

$$\begin{bmatrix} c_4(1) \\ c_4(2) \\ c_4(3) \\ c_4(4) \end{bmatrix} = \begin{bmatrix} c_2(1) & c_2(1) \\ c_2(1) & \overline{c_2(1)} \\ c_2(2) & c_2(2) \\ c_2(2) & \overline{c_2(2)} \end{bmatrix} = \begin{bmatrix} 1 & 1 & 1 & 1 \\ 1 & 1 & -1 & -1 \\ 1 & -1 & 1 & -1 \\ 1 & -1 & -1 & 1 \end{bmatrix}$$

$$\bullet$$

$$\bullet$$

$$\begin{bmatrix} c_N(1) \\ c_N(2) \\ . \\ . \\ c_N(N-1) \\ c_N(N) \end{bmatrix} = \begin{bmatrix} c_{N/2}(1) & c_{N/2}(1) \\ c_{N/2}(1) & \overline{c_{N/2}(1)} \\ . & . \\ . & . \\ c_{N/2}(N/2) & c_{N/2}(N/2) \\ c_{N/2}(N/2) & \overline{c_{N/2}(N)} \end{bmatrix} \qquad \textbf{(2.3)}$$

In the above matrix notation, an over bar indicates binary complement (e.g. $\bar{1} = -1$ and $\overline{-1} = 1$) and N is an integral power of two.

The OVSF codes do not have a single, narrow auto-correlation peak as shown in figure 2.6. As a consequence code-synchronization may become difficult. OVSF codes exhibit perfect orthogonality only at zero lags and even this does not hold for partial-sequence cross-correlation. As a result the advantage of using OVSF codes is lost when all the users are not synchronized to a single time base or when significant multipath is present.

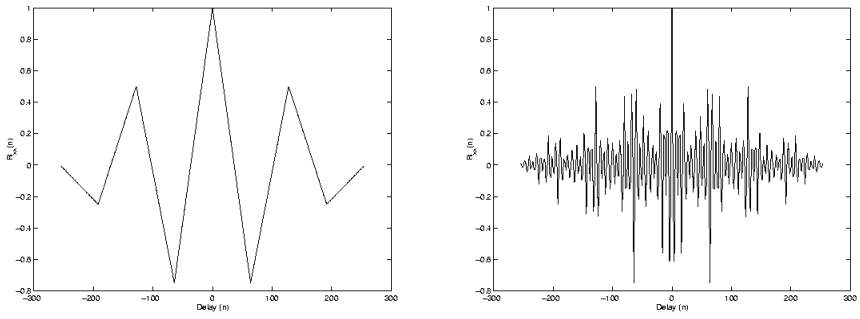

Figure 2.6: Auto-correlation for Two OVSF Codes of SF=256

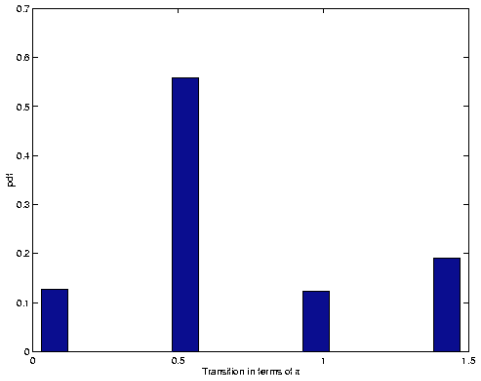

Figure 2.7 a: pdf of Transition in the Signal Constellation with Proper Code Selection

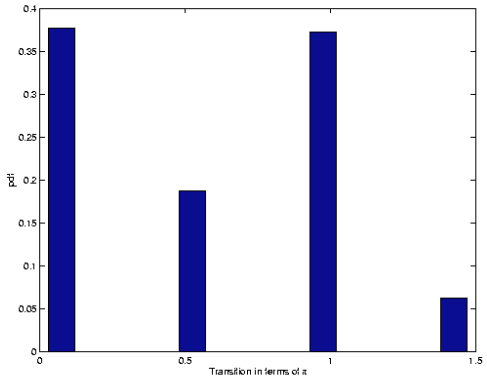

Figure 2.7b: pdf of Transition in the Constellation for Arbitrary Code Selection

The first code of any code tree as described in this section is used to spread the DPCCH. This is a sequence of all 1's for any SF. The first DPDCH is spread by the code number (SF/4+1) where SF is the spreading factor for the data channel. As for example, the 5^{th} code is used for spreading the first DPDCH for a spreading factor of 16. So the spreading code for the first DPDCH is always a repetition of {1,1, -1, -1}. Subsequently added DPDCHs for multi-code transmission are spread by codes in ascending order starting from code number 2 excepting the code used for the first DPDCH. Code selection in this orderly manner along with the proper choice of scrambling code increases the spectral efficiency by limiting the diagonal transitions in the signal constellation. This also results into efficient use

of the power amplifier. Figures 2.7(a) and 2.7(b) show the probability density function of the transitions in the signal constellation of the scrambled signal. The transition of π indicates a diagonal transition in the signal constellation. As we can observe, proper selection of the spreading code can reduce the diagonal transitions in the signal constellation by a significant amount.

2.5 Uplink Scrambling Codes

Uplink Scrambling codes help maintain separation among different mobile stations. Either short or long scrambling codes can be used in the uplink. Short scrambling codes are recommended for base stations equipped with advanced receivers employing multiuser detection or interference cancellation. Since we employed a simple rake receiver, we used long scrambling codes in the simulator.

Scrambling codes (both short and long) can be defined with the help of the following equation

$$C_{sc} = C_1(w_1 + jw_2C_2^{'}) \qquad \textbf{(2.4)}$$

Here, C_1 is a real chip rate code;

$C_2^{'}$ is a decimated version of a real chip rate code C_2.

The usual decimation factor is 2 so that,

$$C_2^{'}(2k) = C_2^{'}(2k+1) = C_2(2k) \qquad \textbf{(2.5)}$$

w_1 is a repetition of {1 1} at the chip rate

w_2 is a repetition of {1 -1} at the chip rate

So we can write

$$C_{sc} = C_1 + jw_2C_1C_2^{'} \qquad \textbf{(2.6)}$$

The following block diagram shows the implementation of equation (2.6). All the addition and multiplication are performed in modulo 2 arithmetic.

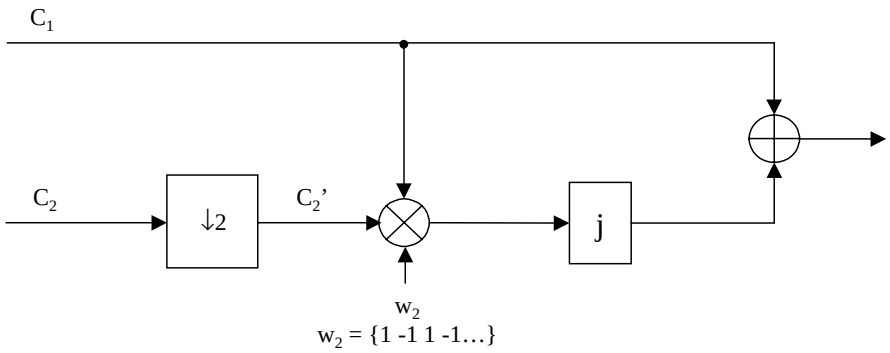

Figure 2.8: Generation of Scrambling Codes

There are two different choices for the period of the scrambling codes. ETSI supports a period of 10 ms or 1 frame where as the ARIB proposal calls for a period of 36864 radio frames or 2^9 super frames. We followed the ETSI proposal as it makes the implementation of our simulator easier.

2.5.1 Uplink Long Scrambling Codes

Long scrambling codes are constructed as described in section 2.5. The real chip rate codes C_1 and C_2 are formed as the position wise *modulo 2* sum of 38400 chip segments of two binary m sequences. The binary m sequences are generated from two generator polynomials of degree 25. This is explained in details below following the discussion in [5]

Two binary sequences *x* and *y* are generated using the generator polynomials $X^{25} + X^3 + 1$ and $X^{25} + X^3 + X^2 + X + 1$ respectively. The resulting sequence constitutes segments of a set of Gold sequences.

Let $n_{23}\ldots\ldots n_0$ be the 24 bit binary representation of the scrambling code number n (decimal). In the binary representation, n_0 is the least significant bit (LSB). The x sequence depends on the choice of the scrambling code number and is thus denoted as x_n. Furthermore, let $x_n(i)$ and $y(i)$ denote the i^{th} symbol of the sequences x_n and y respectively. The m sequences are constructed as

The Initial conditions are set:

$$\begin{aligned} &x_n(0) = n_0, x_n(1) = n_1, \ldots\ldots, x_n(22) = n_{22}, x_n(23) = n_{23}, x_n(24) = 1 \\ &y(0) = y(1) = \ldots\ldots y(23) = y(24) = 1 \end{aligned} \quad \textbf{(2.7)}$$

Then subsequent symbols are generated recursively according to:

$$\begin{aligned} &x_n(i+25) = \left\langle x_n(i+3) + x_n(i) \right\rangle_{\mathrm{mod}\,2}, i = 0,1,\ldots\ldots 2^{25} - 27 \\ &y(i+25) = \left\langle y(i+3) + y(i+2) + y(i+1) + y(i) \right\rangle_{\mathrm{mod}\,2}, i = 0,1,\ldots\ldots 2^{25} - 27 \end{aligned} \quad \textbf{(2.8)}$$

The real chip rate code $C_{1,\mathrm{n}}$ and $C_{2,\mathrm{n}}$ for the nth scrambling code are defined as

$$\begin{aligned} C_{1,n} &= \left\{ \left\langle x_n(0) + y(0) \right\rangle_{\mathrm{mod}\,2}, \left\langle x_n(1) + y(1) \right\rangle_{\mathrm{mod}\,2}, \ldots\ldots, \left\langle x_n(N-1) + y(N-1) \right\rangle_{\mathrm{mod}\,2} \right\} \\ C_{2,n} &= \left\{ \left\langle \begin{matrix} x_n(M) \\ +y(M) \end{matrix} \right\rangle_{\mathrm{mod}\,2}, \left\langle \begin{matrix} x_n(M+1) \\ +y(M+1) \end{matrix} \right\rangle_{\mathrm{mod}\,2}, \ldots, \left\langle \begin{matrix} x_n(M+N-1) \\ +y(M+N-1) \end{matrix} \right\rangle_{\mathrm{mod}\,2} \right\} \end{aligned} \quad \textbf{(2.9)}$$

The scrambling codes are designed so that they have very low cross-correlation among them. This ensures good Multiple Access Interference (MAI) rejection capability. Figure shows a histogram of cross-correlation values for two long scrambling codes.

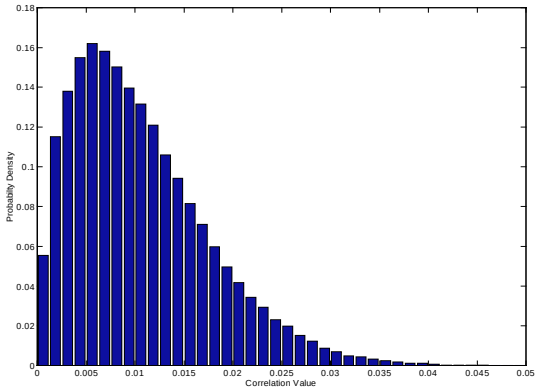

Figure 2.9: Histogram of Cross-correlation of Long Scrambling Codes

2.5.2 Uplink Short Scrambling Codes

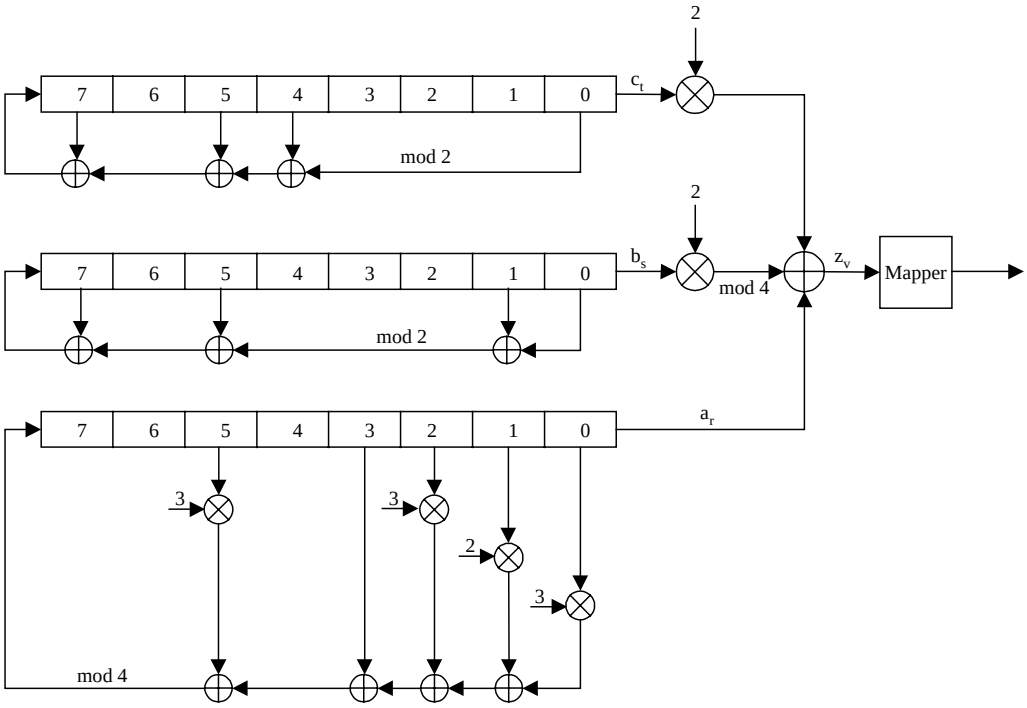

Figure 2.10: Uplink Short Scrambling Code Generator

The short scrambling codes are generated in the same way as described in section 2.5. Here the real and imaginary parts of the complex spreading codes, C_1 and C_2 respectively, are taken from a family of periodically extended $S(2)$ codes. The uplink short codes $S_v(n)$,

n=0,1,..,255, of length 256 chips are obtained as the one chip periodic extension of $S(2)$ sequences of length 255 [5]. So $S_v(0)=S_v(255)$. Figure 2.10 shows the generation of uplink short scrambling codes.

The quaternary sequence $z_v(n)$, $0 \le v \le 16777216$, of length 255 is generated by the modulo 4 summation of the quaternary sequence $a_r(n)$ and the two binary sequences $b_s(n)$ and $c_t(n)$, i.e.

$$z_v(n) = \langle a_r(n) + 2b_s(n) + 2c_t(n) \rangle_{\text{mod } 4} \quad n = 0,1,..,254 \qquad \textbf{(2.10)}$$

The user index v determines the indexes r, s and t in the following way

$$\begin{aligned} v &= r + 2^8.s + 2^{16}.t \\ r &= 0,1,..,254 \\ s &= 0,1,..,254 \\ t &= 0,1,..,254 \end{aligned} \qquad \textbf{(2.11)}$$

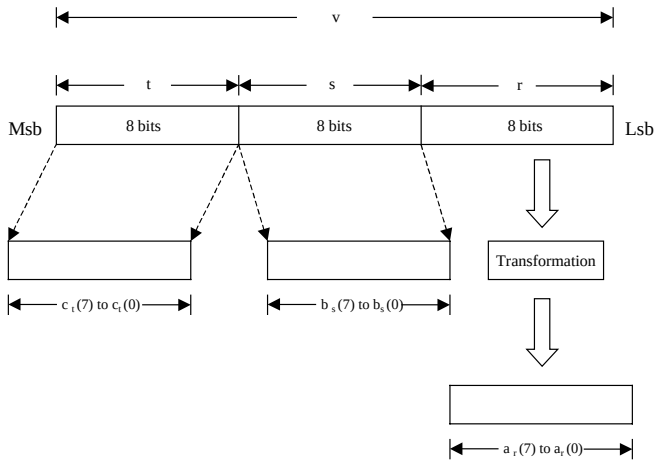

Figure 2.11: Initial Conditions at the Shift Registers

The values of the indexes s and t are converted to 8-bit binary and used as the initial states at the respective registers. The value of the index r is transformed to an 8-bit word before being used as the initial state at the generator. The transformation is given by:

$$a_r(0) = \langle 2v_r(0) + 1 \rangle_{\text{mod}\,4} \quad \textbf{(2.12)}$$

$$a_r(n) = \langle 2v_r(n) \rangle_{\text{mod}\,4} \qquad n = 1,2,..,7 \quad \textbf{(2.13)}$$

Figure 2.11 shows the initial conditions at the shift registers.

The sequence $z_v(n)$ is mapped to $S_v(n)$ according to the following table:

Table 2.1: Mapping of $z_v(n)$

$z_v(n)$	$S_v(n)$
0	+1+j
1	-1+j
2	-1-j
3	+1-j

The real and imaginary parts of $S_v(n)$ are the sequences $C_1(n)$ and $C_2(n)$ respectively.

2.6 Downlink Scrambling Codes

The downlink scrambling codes are used to maintain cell or sector separation. The total number of available scrambling codes is 512. These codes are divided into 32 code groups with 16 codes in each group. The grouping is done to facilitate fast cell search by the mobile [5]. Several scrambling codes might be assigned to one cell for the case adaptive antennas used to increase the capacity.

The downlink scrambling codes are generated in the same way as the uplink scrambling codes. However the generator polynomials are different. As for example the x sequence (similar to that in the uplink) is constructed using the primitive polynomial $1 + X^7 + X^{18}$ and the y sequence is constructed from $1 + X^5 + X^7 + X^{10} + X^{18}$. A detailed

description of the generation of downlink scrambling code is given in [5]. Figure 2.12 shows the generation of downlink scrambling codes:

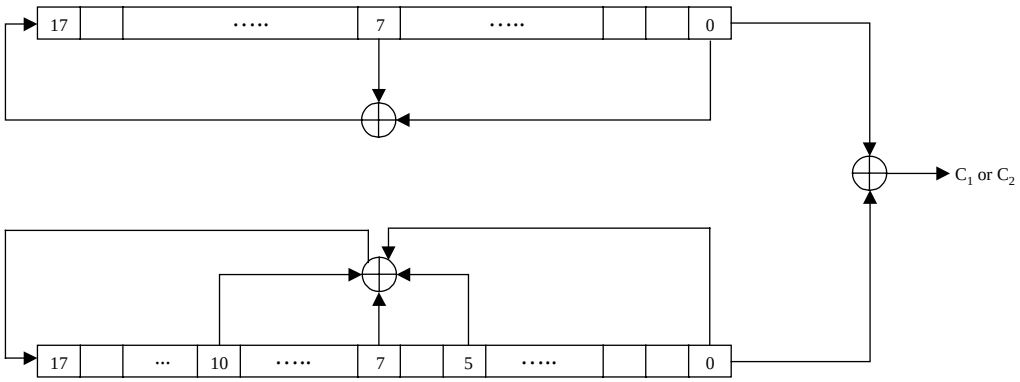

Figure 2.12: Generation of Downlink Scrambling Codes

2.7 Summary of the WCDMA Modulation

We can summarize the discussion on the modulation applied to the dedicated physical channels in the following table

Table 2.2 Parameters of WCDMA Modulation

Spreading Modulation	Dual Channel QPSK for UL Balanced QPSK for DL
Data Modulation	BPSK for UL QPSK for DL
Spreading	OVSF codes. 4-256 spreading factor for UL 4-512 spreading factor for DL
Scrambling	Complex Scrambling
Frame Length	10 ms
Chip Rate	3.84 Mcps
Pulse Shaping	Raised Cosine with 0.22 roll off

2.8 Channel Coding

The main purpose of channel coding is to selectively introduce redundancy into the transmitted data and improve the wireless link performance in the process [9]. Channel codes can be used to detect as well as correct errors. The WCDMA systems have provision for both error detection and error correction. Channel coding scheme at the WCDMA system is a combination of error detection, error correction, along with rate matching, interleaving and transport channels mapping onto/splitting from physical channels [10]. This section gives a brief description on the error detection and error correction schemes recommended for the WCDMA systems.

2.8.1 Error Detection

Error detection is provided by a Cyclic Redundancy Check (CRC) code. The CRC is 24,16,8 or 0 bits. The entire transmitted frame is used to compute the parity bits. Any of the following cyclic generator polynomials can be used to construct the parity bits:

$$\begin{aligned} g_{24}(D) &= D^{24} + D^{23} + D^6 + D^5 + D + 1 \\ g_{16}(D) &= D^{16} + D^{12} + D^5 + D + 1 \\ g_8(D) &= D^8 + D^7 + D^4 + D^3 + D + 1 \end{aligned} \qquad \textbf{(2.14)}$$

A detailed description of the error detection scheme is given in [10].

2.8.2 Error Correction

Two alternative error correction schemes have been specified for the WCDMA system. They are

- Convolutional Coding
- Turbo Coding

For standard services that require BER up to 10^{-3}, which is the case for voice applications, convolutional coding is to be applied. The constraint length for the proposed convolutional coding schemes is 9. Both rate 1/2 and 1/3 convolutional coding has been specified. For high-quality services that require BER from 10^{-3} to 10^{-6}, turbo coding is required. The feasibility of applying 4-state Serial Concatenated Convolutional Code (SCCC) is being investigated by different standardization bodies. Reference [10] provides a detailed description of the error correction coding schemes along with rate matching, interleaving and transport channel mapping.

In chapter 4 we will apply a rate 1/3, constraint length 9 convolutional coding scheme to an uplink 9.6 kbps voice service and show the BER improvement as a result of coding gain.

2.9 Performance Enhancing Schemes

The number of performance enhancing schemes has been proposed for the WCDMA systems. They include adaptive receiving antennas, transmit diversity schemes, and advanced receiver structures [11].

2.9.1 Adaptive Antennas

Adaptive antennas at the receiver can increase the capacity and coverage of the system [12]. Connection dedicated pilot bits can be used in both the links for employing adaptive antennas.

2.9.2 Transmit Diversity Schemes

Transmit diversity schemes at the downlink employ multiple transmit antennas at the base station. They provide performance enhancement similar to that with multiple antennas at the mobile station receivers. These schemes are attractive since they transfer the processing burden to the base station. The transmit diversity schemes proposed for the WCDMA systems fall broadly into two different categories:

- Open Loop
- Closed Loop

In the open loop transmit diversity the techniques are Time Switched Transmit Diversity (TSTD), [6] and Space-Time TD (STTD). A space- time transmit diversity scheme similar to the one proposed by Alamouti [13] has been evaluated in [14]. The closed loop technique includes the feedback mode Transmit Diversity and Selection Transmit Diversity (STD) [15].

2.9.3 Advanced Receiver Structure

WCDMA systems are designed to provide reasonable service quality without using complex receivers that use joint detection of multiple user signals. However if required, short scrambling codes can be used at the uplink to implement multiuser receivers at moderate complexity.

Chapter 3

Simulator Description

This chapter describes the simulator designed to evaluate the Bit Error Rate (BER) at the uplink and the downlink of a Wideband CDMA (WCDMA) system. Data is transmitted in a frame by frame basis over a time varying multipath channel. Receiver design incorporates rake diversity combining. Additive White Gaussian Noise (AWGN) is added at the front end of the rake receiver. Multiple Access Interference (MAI) is generated in a structured way rather than treating it as AWGN. No error correction coding schemes or antenna diversity technique was considered for the basic simulator. However we will show in chapter 4 that the simulator is very flexible and can be modified to incorporate error correction coding.

3.1 Simulator

The simulator consists of two major subsections:

- Uplink Simulator
- Downlink Simulator

As their names indicate, these two subsections implement the uplink and the downlink of the simulator respectively. The major differences between them are:

1. Frame structure
2. The way Multiple Access Interference (MAI) is added to the signal of the desired user

These differences will become evident as we describe the simulator in the subsequent sections. The following sections contain a detailed description of the WCDMA simulator.

3.2 Uplink Simulator

At the uplink, the base station receiver receives signals from all the mobile station transmitters and demodulates them. The signals from different MS follow different channels to reach the base station. The block diagram of the uplink simulator is shown in figure 3.1.

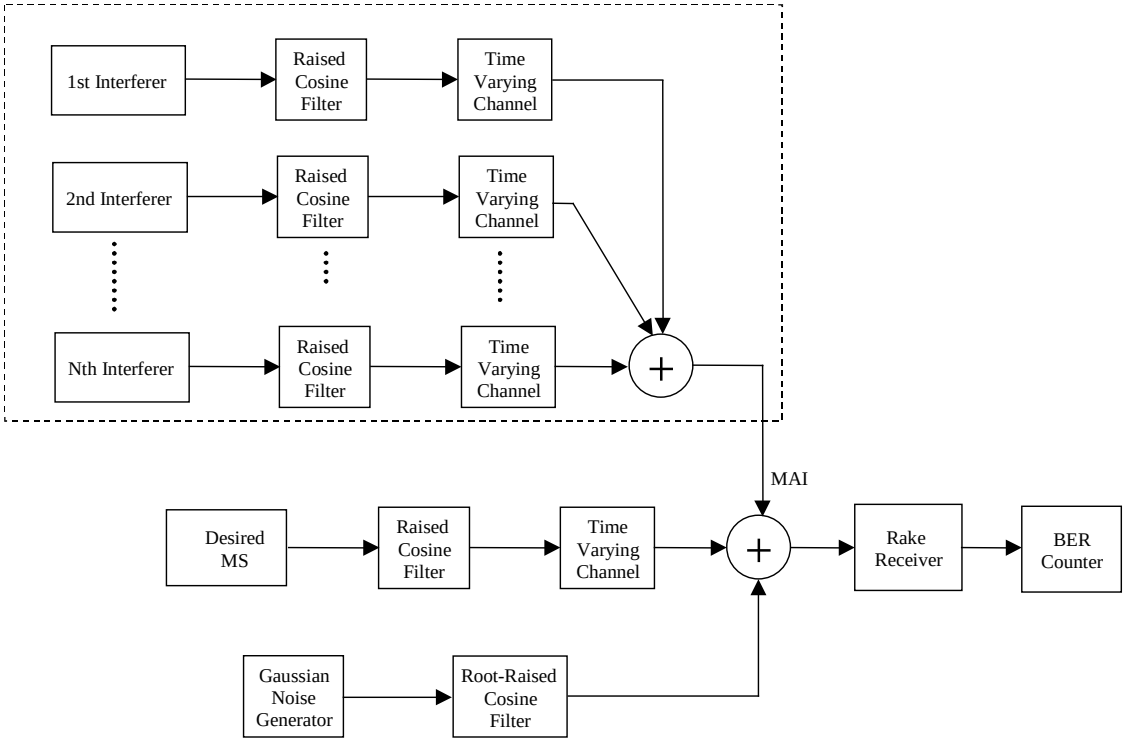

Figure 3.1: Uplink Simulator

The following sub-sections describe each block of the uplink simulator.

3.2.1 Desired MS

The desired MS is the user for which the simulator estimates the BER. The desired user has a dedicated control channel and one data application as shown in Figure 3.2. The

noise variance is calibrated according to the spreading factor of the data channel and the BER is evaluated for the data channel only.

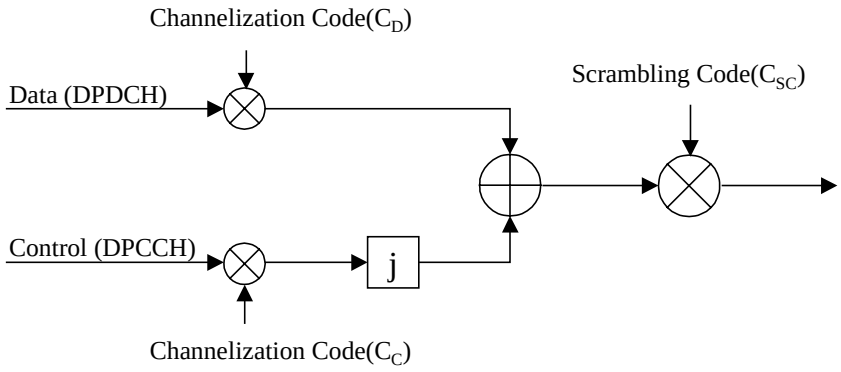

Figure 3.2: Desired MS

The channelization codes C_D and C_C are chosen as described in section 2.4. The scrambling code is an MS specific long code with a period of one frame or 10 ms, as described in section 2.5.

3.2.2 Multiple Access Interference

MAI is implemented by generating the signals for a number of interfering MS within the system. Each interfering user has its own control channel and one data application. Each of the interfering mobile station generates its transmitted frame in the same manner as the desired user. However these frames are not aligned in time with each other or with that of the desired MS. The maximum offset between the frames of an interfering user and that of the desired user can be calculated in the following way:

Let the cell radius be D km.

The maximum offset between the frames of a user and an interferer is the time taken by signal to make a round trip of D+D = 2D km. This time is given by

$$t_{offset} = \frac{2D}{c} \quad \textbf{(3.15)}$$

Here c is the velocity of light. If we assume a cell radius of 20 km we get

$$t_{offset} = \frac{2 \times 20 \times 10^3}{3 \times 10^8} = \frac{4}{3} \times 10^{-4} \text{ Sec} \quad \textbf{(3.16)}$$

Since we have a chip rate of 3.84 Mcps, the maximum offset corresponds to $\frac{4}{3} \times 10^{-4} \times 3.84 \times 10^6 = 512$ chips.

These asynchronous transmitted frames arrive at the base station via different multipath channels and constitute MAI. In this simulator we assume that we have perfect power control (i.e. all the users transmit at equal power and the received signal at the base station for all the users are at the same average power level).

3.2.3 Time Varying Channel

The chip rate of the WCDMA signal is 3.84 Mcps. This narrow pulse width means that the multipaths would be resolved most of the time and the transmitted signal will encounter frequency selective fading. Three different types of multipath channel were employed in the simulator. They are

1. Indoor channel
2. Indoor to Outdoor channel
3. Vehicular A Outdoor channel

However, different channel models like COST 207 [16] or Simple Two Ray Model [17] can also be easily incorporated with the simulator.

Each of the three channels employed at the simulator corresponds to different environment as their names suggest. The multipath profiles of the channels shown in the

following tables are taken from [11], and contain a series of specular components with the relative delays and amplitudes indicated.

Table 3.1a Indoor Channel Power Delay Profile

Relative Delay	Avg. Power
0	0
50	-3
110	-10
170	-18
290	-26
310	-32

Table 3.1b Indoor to Outdoor Channel Power Delay Profile

Relative Delay	Avg. Power
0	0
110	-9.7
190	-19.2
410	-22.8

Table 3.1c Vehicular A Outdoor Channel Power Delay Profile

Relative Delay	Avg. Power
0	0
310	-1
710	-9
1090	-10
1730	-15
2510	-20

All the delays in the tables are measured at nano-secs and the power is shown in dB scale. The vehicular A channel has a mobile speed of 120 Km per hour associated with it where as the other two channels correspond to a pedestrian walking speed of 5 Km per hour. A mobile speed of 120km/h corresponds to a Doppler spread of 223 HZ for a carrier frequency of 2 GHz This is very small compared to the bandwidth of the baseband signal and represents a relatively slow fading environment.

The multipath channel profiles are converted to the time resolution of the simulation model in the following way [11]:

Each ray is split into two rays, one to the sample to the left and one to the sample to the right. The power of these new rays is such that the sum is equal to the original power, and the power of each of the new rays is inversely proportional to the distance of the original ray. The power of all the rays on one sample are added up and normalized. This is graphically demonstrated in figure 3.3.

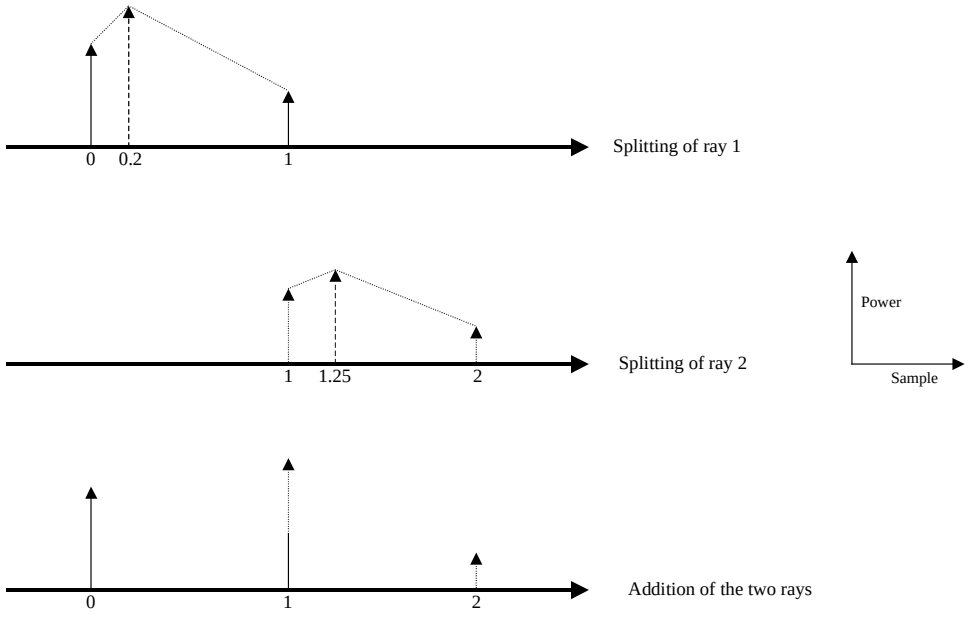

Figure 3.3: Equivalent Channel Model

The ideal way to convert the multipath profiles to the time resolution of the simulation is to perform an interpolation with a $\frac{\sin(x)}{x}$ function (sinc) (i.e. employing an ideal brick-wall low pass filter). But in that situation, we will have a channel profile with a large number of multipath components. Since each of the paths is individually Rayleigh faded; this will increase the simulation run time significantly. With the simple interpolation method employed in the simulator, we have a small number of non-zero components in the reconstructed multipath profile. There is a loss of information in the interpolation process.

But if the sampling rate is high enough (4 samples per chip and above) the interpolated channel response follows that of the original channel very closely in the frequency band of interest. This is demonstrated in the following figures

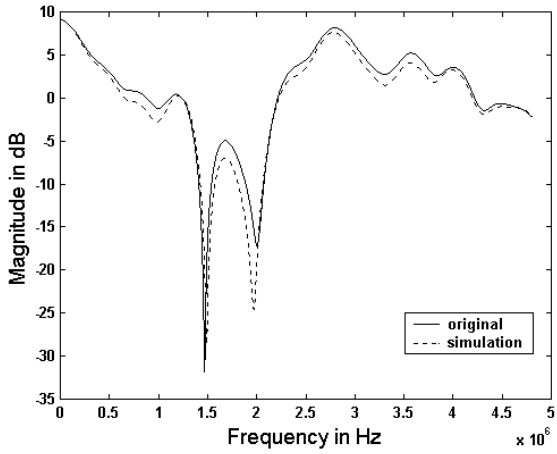

Figure 3.4a: Frequency Response of the Vehicular A Outdoor Channel. (Simulation Resolution is 5 Samples per Chip)

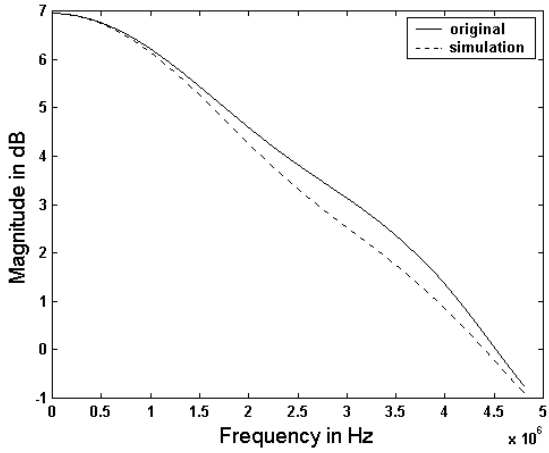

Figure 3.4b: Frequency response of the Indoor Channel. (Simulation Resolution is 5 Samples per Chip)

The pass-band of the pulse shaping filter is the band of interest in the simulator. The channel coefficients are normalized so that $\sum_{k=1}^{N} h_k^2 = 1$, where we have N channel coefficients. This normalization ensures that the average signal energy at both end of the channel remains the same. This allows us to take the energy of the signal at the transmitter as the received signal energy (E_b) during the estimation of receiver front end E_b/N_0 value.

The channels used in the simulator are linear time variant filters. We have a number of independently Rayleigh faded components on the sampling instants. Figure 3.5 shows the block diagram of the time varying channel

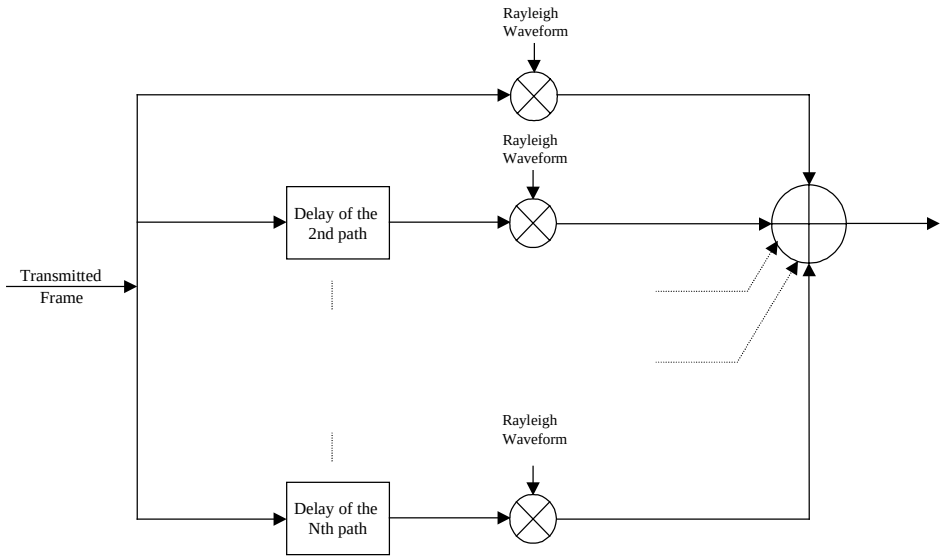

Figure 3.5: Time Varying Channel

The delays are implemented by treating each the transmitted data block (a frame of 10 ms for the simulator) in a circular fashion. To implement a delay of τ samples, the last τ samples of a transmitted frame are taken out. This block of τ samples is then added to the beginning of the truncated transmitted data block. This is shown in the Figure 3.6.

The Rayleigh waveform is generated using Clarke's model [9]. Complex Normal noise samples, which are uncorrelated in the time domain, are passed through a Doppler

filter. This Doppler filter imparts correlation to the time domain samples according to the Doppler spread. The Doppler spread is a function of the mobile speed. The waveform coming out of the Clarke's model waveform generator has a Rayleigh amplitude distribution and a uniform phase distribution between [0,2π]. The mean value of the amplitude is unity. We multiply this waveform by the amplitude of the corresponding path and use that as the Rayleigh waveform in the time varying channel of figure 3.5.

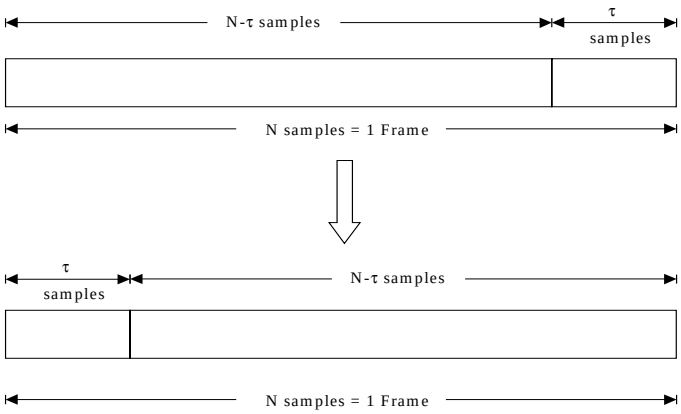

Figure 3.6: Implementation of Delay of τ Samples

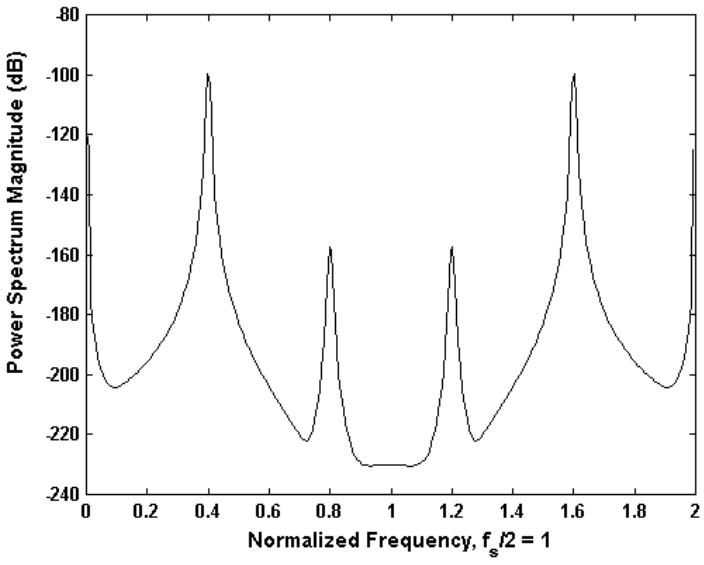

Figure 3.7: Interpolation Noise in the Rayleigh Waveform. (The Factor of Interpolation is Five)

The Rayleigh waveform is generated at a sampling rate equal to the chip rate. Samples for higher sampling rate is constructed by interpolation. This reduces the simulation time significantly at the expense of an injection of a small amount of noise. The noise generated as a result of interpolating the Rayleigh waveform is insignificant as shown in Figure 3.7.

The Rayleigh waveform can be generated at the symbol rate rather than at the chip rate. This will reduce the simulation run time even more. Even for a relatively large Doppler spread of 223 Hz which corresponds to a mobile speed of 120 km/h, the interpolation noise remains below –30 dB for the worst case scenario of a sampling factor of 8 and a spreading factor of 256. This noise does not cause any measurable change in the BER.

3.2.4 Addition of Noise

The Additive White Gaussian Noise (AWGN) added at the front end of the receiver is generated by a Gaussian random number generator. The variance of the noise distribution depends on the Signal to Noise Ratio (SNR) or $\frac{E_b}{N_0}$ at the receiver front end. The noise variance is also a function of the spreading factor, signal amplitude and sampling rate i.e. the number of samples per chip. The calibration of noise is discussed in the following section.

3.2.4.1 Calibration of Noise

Let us assume for the time being that no pulse shaping is employed. Figure 3.8a and 3.8b show the chip and the double sided noise spectrum.

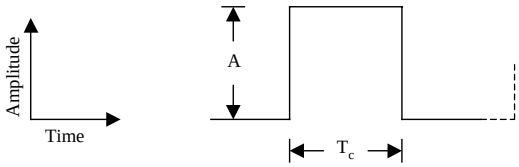

Figure 3.8a: Chip

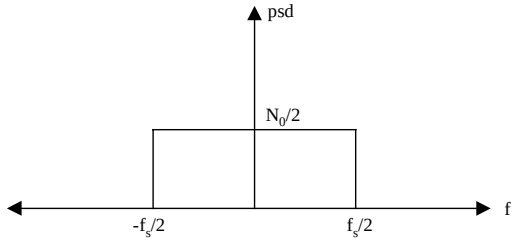

Figure 3.8b: Noise Spectrum

Here,

Duration of chip: T_c

Amplitude of chip: A

Sampling rate: f_s

Noise power spectral density: N_0

The energy per chip

$$E_c = A^2 T_c \tag{3.17}$$

If the spreading factor is *SF* then the energy per bit

$$E_b = SF \times E_c = (SF) A^2 T_c \tag{3.18}$$

The noise variance is given by

$$\sigma^2 = \frac{N_0 f_s}{2} \tag{3.19}$$

$$\therefore \frac{E_b}{N_0} = \frac{(SF) A^2 T_c}{2\sigma^2 / f_s} = \frac{(SF) A^2 (T_c f_s)}{2\sigma^2} \tag{3.20}$$

But $T_c f_s$ is equal to the number of samples per chip, *m*.

So,

$$\frac{E_b}{N_0} = \frac{(SF) A^2 m}{2\sigma^2}$$
$$\Rightarrow \sigma^2 = \frac{(SF) A^2 m}{2(E_b / N_0)} \tag{3.21}$$

This expression can be used directly if rectangular pulse shaping is assumed and we integrate or sum all the samples in a chip to make a decision on the chip at the receiver. However we have to be careful about evaluating noise variance when Raised Cosine pulse shaping is assumed. If at the receiver we sample at the chip rate to reconstruct each chip, we must use $m = 1$ in equation (3.7). This is because we are using one sample not m samples for making a decision on the chip.

3.2.5 Pulse Shaping

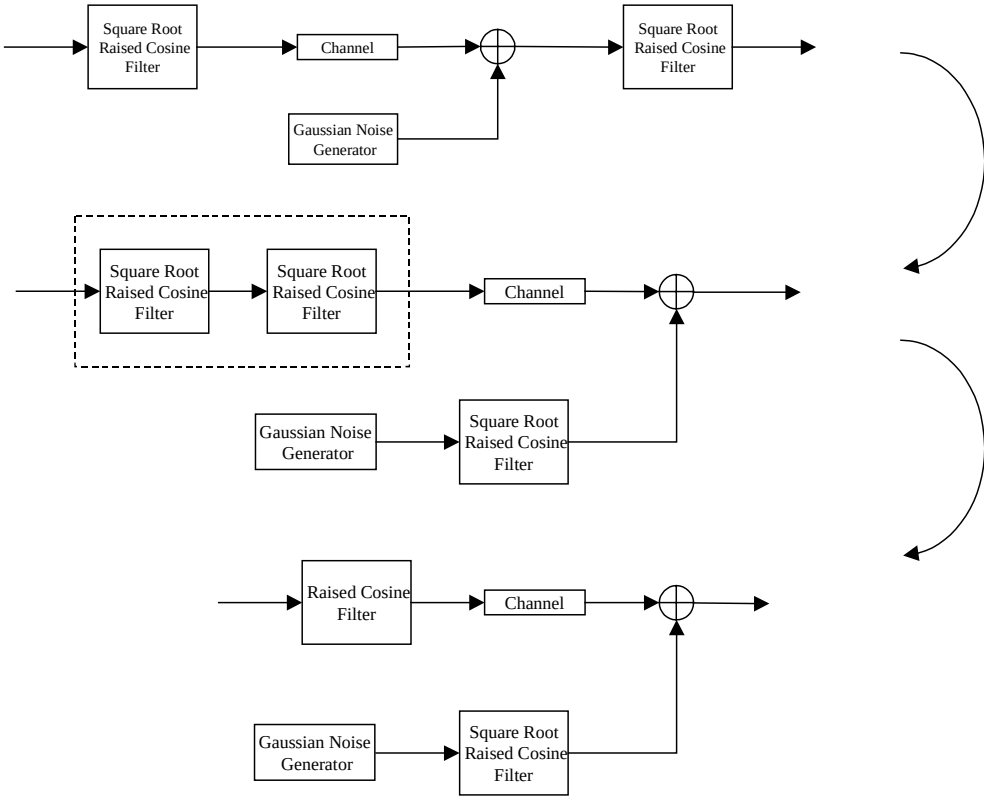

1 Figure 3.9: Implementation of Pulse shaping and Gaussian Noise

Data is pulse shaped through a Square Root Raised Cosine (Root RC) filter at the transmitter. The receiver at the base station has a filter matched to the pulse shaping filter at the transmitter. Both these filters have a roll-off of 0.22. In the simulator the transmitter and

the receiver filters are cascaded and they constitute a Raised Cosine (RC) filter. The noise has to be passed through a Root RC filter before it is added to the received frame. This rearrangement is shown in Figure 3.9. The noise variance is calculated as described in section 3.2.4.1.

Only the first three lobes of the Raised Cosine were considered for implementing the filters and all the filters were implemented as symmetric FIR filters. Symmetric FIR filters have a delay equal to half the order of the filter. So to take this delay into account we padded each transmitted data block by an additional data segment whose size is equal to the delay. So if the delay of the filter is N_D samples we repeated the first N_D samples of the data at the end of the data block. After the filtering, we removed the first N_D output of the filter. We ignored the transient of the filter. However the transient can be easily removed by passing a smaller data block through the filter and store the state before passing the data frame for pulse shaping.

3.2.6 Rake Receiver

Multipath is resolved for WCDMA system because of the wide bandwidth. Rake receiver [18] is used to exploit the consequent time diversity. The default number of fingers at the base station receiver is four. However any number of finger between three and six can be chosen. The simple case of one finger is also provided as an option. The block diagram shown in Figure 3.10 illustrates the implementation of the rake receiver. It is assumed that the receiver has perfect channel estimation. Maximal Ratio Combining (MRC) is employed for rake combining [19], [20].

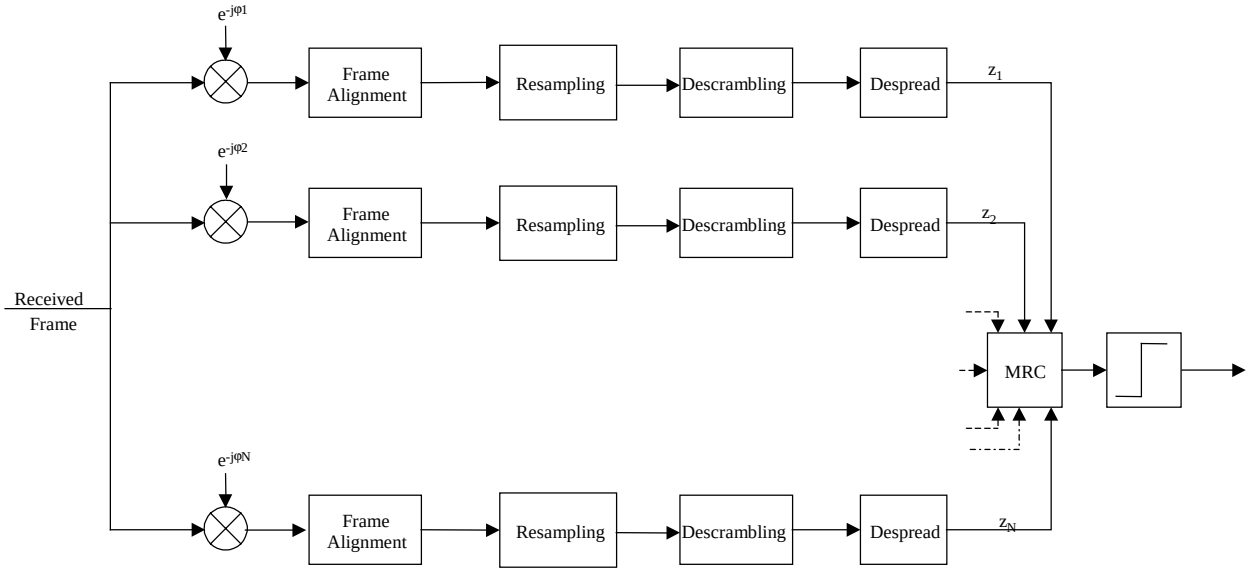

2 Figure 3.10: Rake Receiver

3.2.6.1 Description of the Rake Receiver

When a frame is transmitted through the time varying channel, it is multiplied with independent Rayleigh faded waveforms along each path. These time varying waveforms are complex. The amplitude distribution is Rayleigh and the phase distribution is uniform in the interval $[0,2\pi]$. The phase associated with the Rayleigh waveform rotates the constellation of the transmitted signal. So in the rake receiver we cancel the rotation by multiplying the received frame in each branch by the negative of the phase associated with that particular path. We assume that we have perfect phase estimation so that we can cancel out the phase in each branch.

The frame alignment block takes care of the delay associated with each path so that we know the frame boundary at each branch. We then reconstruct each chip from the pulse shaped signal by sampling at the chip rate. This is performed in the Resampling block. Descrambling is performed by multiplying the resampled signal by the complex conjugate of

the desired MS specific scrambling code. The following figure illustrates the descrambling process

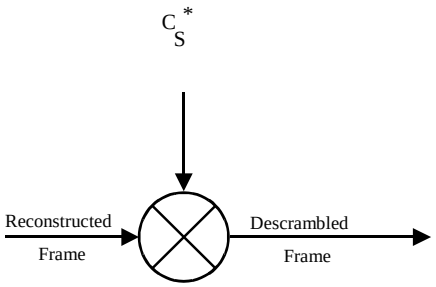

3 Figure 3.11: Descrambling

C_S is the scrambling code of the desired Mobile Station in the uplink. It represents the scrambling code of the desired base station in the downlink simulator. The asterisk (*) indicates complex conjugation. Figure 3.12 shows the despreading operation,

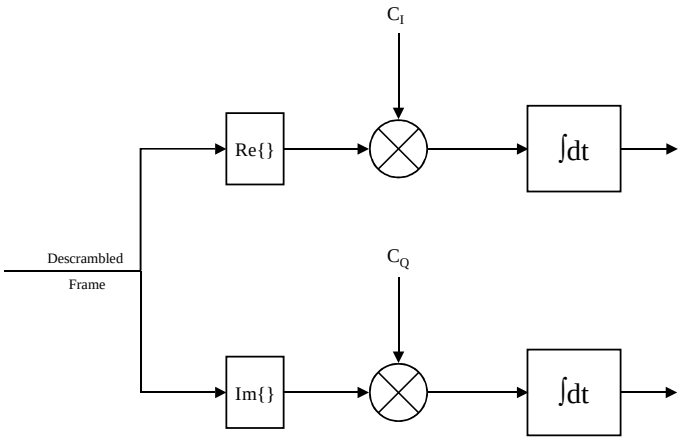

4 Figure 3.12: Despreading

where C_I and C_Q represent the appropriate spreading codes in figure 3.12.

The despread decision statistic from each branch is combined and a hard decision is made on the bit. Maximal Ratio Combining (MRC) is employed. We assume that we have perfect amplitude estimate of the channel while estimating the weights for MRC.

3.2.7 BER Counter

The bit error rate counter compares the decision of the hard-limiter for the I channel or the data channel to the transmitted data at the I channel and counts the number of error. BER is evaluated by averaging the number of error over several transmitted frames. At least 400 frames are used to compute the BER at low SNR. To compute the BER at higher SNR, as many as 4000 frames were used.

3.2.8 Analytical Treatment of the Uplink Simulator

Let us assume for the time being that no MAI is present in the system. The following figure shows the transmitter and the signals at different points.

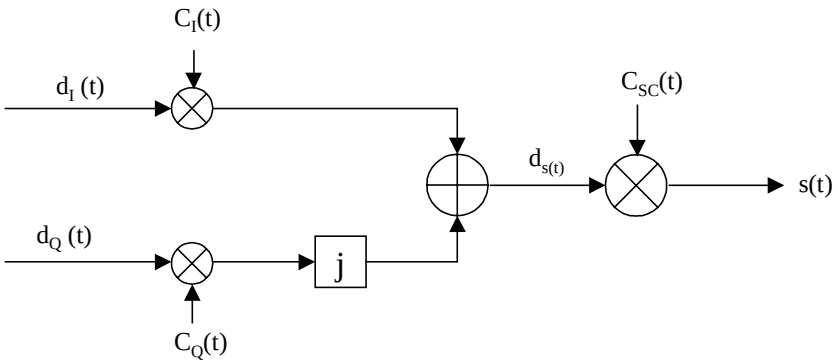

Figure 3.13: Transmitter

The data at the I channel is represented by the signal $d_I(t)$, while the data at the Q channel is represented by $d_Q(t)$.

The spread data is denoted as,

$$d_s(t) = d_I(t)c_I(t) + jd_Q(t)c_Q(t) \qquad \textbf{(3.22)}$$

c_I and c_Q are I and Q channel spreading codes respectively.

Finally the transmitted data is given by,

$$s(t) = d_s(t)c_{sc}(t) \qquad \textbf{(3.23)}$$

where c_{SC} is the complex uplink scrambling code as described in section 2.5.

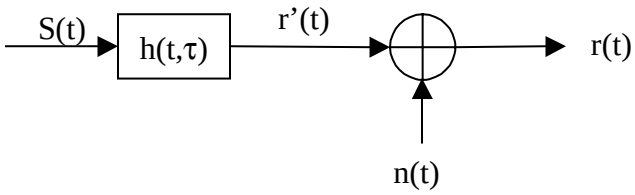

Figure 3.14: Transmission through Channel and Reception at the Rake Front End

Each transmitted signal is passed through a multipath channel as shown in Figure 3.14, where

$r(t)$ is the received signal

$h(t,\tau)$ is the complex channel response

$n(t)$ is the complex Gaussian noise at the front end of the receiver

Now,

$$r'(t) = \sum_{i=1}^{N} h_i(t,\tau_i)s(t-\tau_i) \qquad \textbf{(3.24)}$$

Here we assume that we have N multipath component in the channel. Each of these $h_i(t,\tau_i)$ is complex i.e. $h_i(t) = |h_i(t,\tau_i)|e^{j\phi_i(t,\tau_i)}$

The received signal is then given by,

$$r(t) = r'(t) + n(t) \qquad \textbf{(3.25)}$$

The following figure represents the signals at the i^{th} finger of the rake receiver.

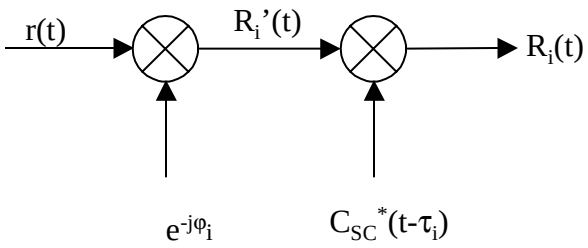

Figure 3.15: Descrambling at a Rake Branch

$$\begin{aligned} R_i^{'}(t) &= r(t)e^{-j\phi_i(t)} \\ &= \{r'(t)+n(t)\}e^{-j\phi_i(t)} \\ &= r'(t)e^{-j\phi_i(t)} + n(t)e^{-j\phi_i(t)} \end{aligned} \quad \textbf{(3.26)}$$

The second term in equation (3.12) is the complex Gaussian noise with a rotation. Let us denote that as $n_i'(t)$. So,

$$\begin{aligned} R_i^{'}(t) &= r'(t)e^{-j\phi_i(t)} + n_i(t) \\ &= \sum_{l=1}^{N} |h_l(t-\tau_l)| s(t-\tau_l)e^{j\phi_l(t)}e^{-j\phi_i(t)} + n_i^{'}(t) \\ &= |h_i(t-\tau_i)| s(t-\tau_i) + \sum_{\substack{l=1 \\ l\neq i}}^{N} |h_l(t-\tau_l)| s(t-\tau_l)e^{j\phi_l(t)}e^{-j\phi_i(t)} + n_i^{'}(t) \end{aligned} \quad \textbf{(3.27)}$$

The first term in equation (3.13) is the desired signal. Let us call that $m_i'(t)$. The second term is interference due to other paths or the Inter Symbol Interference (ISI). Let us denote that as $I_i'(t)$. So we have

$$R_i^{'}(t) = m_i^{'}(t) + I_i^{'}(t) + n_i^{'}(t) \quad \textbf{(3.28)}$$

$$\begin{aligned} \therefore R_i(t) &= R_i^{'}(t)C_{SC}^{*}(t-\tau_i) \\ &= m_i^{'}(t)C_{SC}^{*}(t-\tau_i) + I_i^{'}(t)C_{SC}^{*}(t-\tau_i) + n_i^{'}(t)C_{SC}^{*}(t-\tau_i) \end{aligned} \quad \textbf{(3.29)}$$

The first term representing the desired signal $m_i(t)$ is given by

$$\begin{aligned} m_i(t) &= m_i^{'}(t)C_{SC}^{*}(t-\tau_i) \\ &= |h_i(t-\tau_i)| s(t-\tau_i)C_{SC}^{*}(t-\tau_i) \\ &= |h_i(t-\tau_i)| d_s(t-\tau_i)C_{SC}(t-\tau_i)C_{SC}^{*}(t-\tau_i) \\ &= |h_i(t-\tau_i)| d_s(t-\tau_i) \end{aligned} \quad \textbf{(3.30)}$$

The second term representing the ISI $I_i(t)$ is given by

$$\begin{aligned} I_i(t) &= \sum_{\substack{l=1 \\ l\neq i}}^{N} |h_l(t-\tau_l)| s(t-\tau_l) e^{j\{\phi_l(t)-\phi_i(t)\}} C_{SC}^*(t-\tau_i) \\ &= \sum_{\substack{l=1 \\ l\neq i}}^{N} |h_l(t-\tau_l)| d_s(t-\tau_i) C_{SC}(t-\tau_l) C_{SC}^*(t-\tau_i) e^{j\{\phi_l(t)-\phi_i(t)\}} \end{aligned} \quad \textbf{(3.31)}$$

The third term representing the noise $n_i(t)$ is given by

$$n_i(t) = n_i'(t) C_{SC}^*(t-\tau_i) \quad \textbf{(3.32)}$$

The following figure shows the despreading process

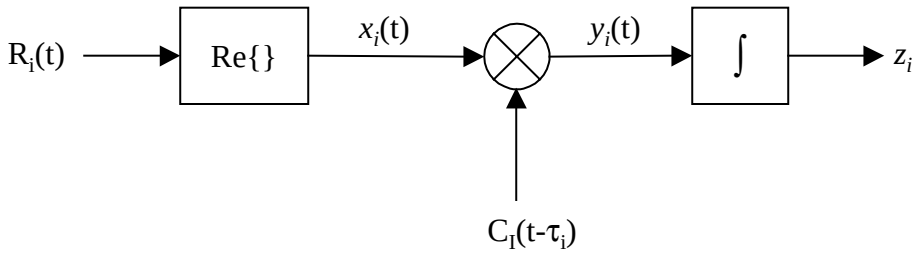

Figure 3.16: Despreading at a Rake Branch

Here z_i is the decision statistic for the i^{th} branch of the rake receiver. Now,

$$\begin{aligned} x_i(t) &= \mathrm{Re}\{R_i(t)\} = \mathrm{Re}\{m_i(t)\} + \mathrm{Re}\{I_i(t)\} + \mathrm{Re}\{n_i(t)\} \\ &= |h_i(t-\tau_i)| d_I(t-\tau_i) C_I(t-\tau_i) + \mathrm{Re}\{I_i(t)\} + \mathrm{Re}\{n_i(t)\} \end{aligned} \quad \textbf{(3.33)}$$

Therefore

$$\begin{aligned} y_i(t) &= x_i(t) C_I(t-\tau_i) \\ &= |h_i(t-\tau_i)| d_I(t-\tau_i) + \mathrm{Re}\{I_i(t)\} C_I(t-\tau_i) + \mathrm{Re}\{n_i(t)\} C_I(t-\tau_i) \end{aligned} \quad \textbf{(3.20)}$$

So the decision statistic z_i is given by

$$z_i = \int_{\tau_i}^{T+\tau_i} y_i(t)\,dt \quad \textbf{(3.21)}$$

which may be evaluated as

$$z_i = \int_{\tau_i}^{T+\tau_i} |h_i(t-\tau_i)| d_I(t-\tau_i)dt + \int_{\tau_i}^{T+\tau_i} \mathrm{Re}\{I_i(t)\}C_I(t-\tau_i)dt + \int_{\tau_i}^{T+\tau_i} \mathrm{Re}\{n_i(t)\}C_I(t-\tau_i)dt \quad \textbf{(3.22)}$$

Here T is the symbol period. If we assume that the magnitude response of the channel remains constant for the symbol interval, we get

$$z_i = T|h_i|K + \int_{\tau_i}^{T+\tau_i} \mathrm{Re}\{I_i(t)\}C_I(t-\tau_i)dt + \int_{\tau_i}^{T+\tau_i} \mathrm{Re}\{n_i(t)\}C_I(t-\tau_i)dt \quad \textbf{(3.23)}$$

Here K can be either 1 or –1 depending on the transmitted symbol. The second term in equation (3.22) is ISI. Because of the processing gain, the ISI is pretty small compared the first tem of the equation (3.22). The third term here is the noise term.

The above analysis can be extended to take the presence of MAI into account. Equation (3.22) will be modified as a fourth term corresponding to MAI will be added.

3.3 Downlink Simulator

At the downlink, the mobile station receiver receives the signal transmitted by the base station transmitter. The MS receives the desired signal along with signals transmitted by the base station for other mobile stations at the system. The block diagram of the downlink simulator is shown in Figure 3.17.

The downlink simulator differs from the uplink simulator in the generation of MAI. The frame structure and the spreading and modulation are a also modified from the up link.

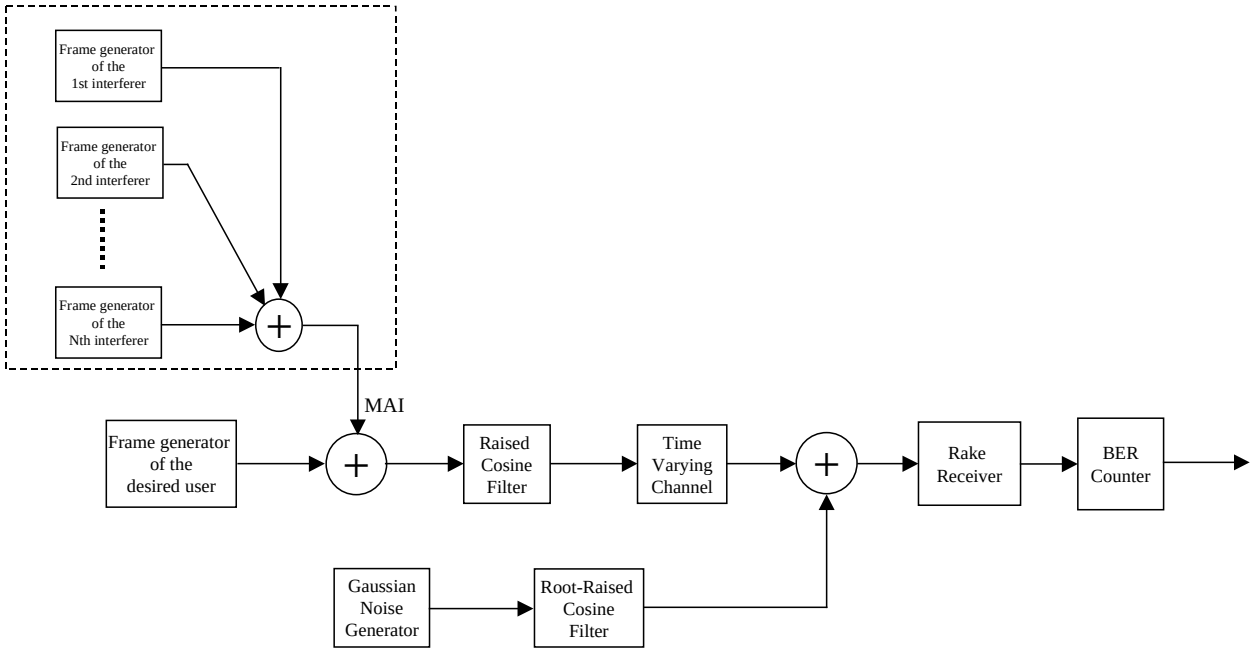

Figure 3.17: Block Diagram of the Downlink Simulator

3.3.1 Downlink Transmitter

Data and control bits are time multiplexed at the transmitter that is a base station for the downlink. The modulation structure for the downlink is shown in Figure 3.18.

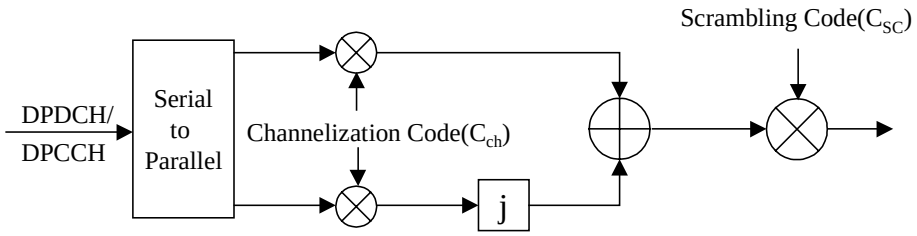

Figure 3.18: Downlink Modulation

The channelization code is the same as described in section 2.4. The scrambling code is base station specific long code with a period of one frame or 10 ms.

3.3.2 MAI for Downlink

The MAI in the downlink arises from data frames transmitted by the base station transmitter for other users in the system. These frames are modulated in a similar manner of Figure 3.18. Each user has its own OVSF code that provides orthogonality among different users. The frames are time aligned with each other and with that of the desired user. They experience the same multipath channel as the data frame of the desired user. This is in contrast with the uplink where the data from different users reaches the receiver via different channel. As a result the MAI is implemented in the following way:

Additional interfering data frames are generated along with the frame for the desired user. They are summed up with the frame of the desired user, passed through the pulse-shaping filter and subsequently received at the desired MS after going through the time varying channel. We assume the frames of all are transmitted at equal power.

3.3.3 BER Counter for Downlink

Unlike the uplink simulator, bit error rate is counted for both the I and Q channels. The mean of this error (for one frame) is averaged over several frames to evaluate the BER.

3.4 Graphic User Interface (GUI) for the Simulator

The description of the GUI for the simulator is presented in this section. The menu driven interactive GUI includes both the uplink and downlink simulators. For each of the simulators, the user can either select the default values for the parameters or can provide values of his choice. The main menu can be called by typing in the word *wcdma* at the Matlab command prompt. This generates a window as shown in figure 3.19.

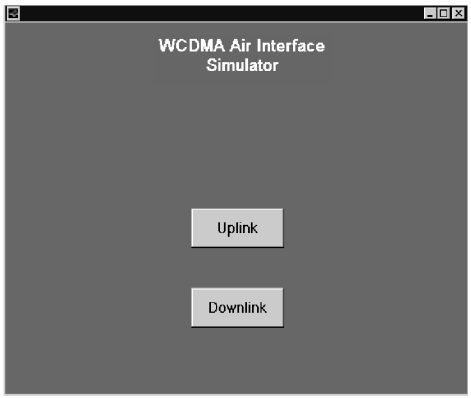

Figure 3.19: Main Interface

Then the user can choose either the downlink or uplink simulator by pressing the appropriate buttons. Pressing the uplink button will cause the menu for the uplink simulator to appear on the screen as shown in figure 3.20.

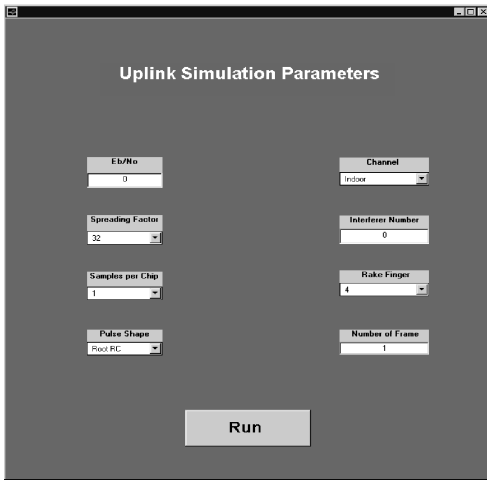

Figure 3.20 Interface for Uplink Simulator

The uplink simulator provides the user with various parameters describing the overall system design. The user can select the parameter E_b/N_0. This can be single value or an array. While giving the values to the simulator, MATLAB syntax has to be followed. For parameters such as spreading factor, samples per chip, channel and number of rake fingers there are pull-down menus that provide the user with the valid ranges or values for the particular parameter. Although Raised Cosine pulse shaping is the standard, a pull-down

menu is provided which gives the option for rectangular pulse shaping as well as Raised Cosine filtering. The number of interferers has to be typed in the corresponding text box. The number of frame parameter determines how many frames the simulator will process before generating an output. Each of these parameters has their default settings as shown in the next table:

Table 3.2: Default Parameters for the Uplink Simulator

Eb/N0 (dB)	5
Spreading Factor	32
Samples per Chip	1
Pulse Shape	Raised Cosine
Channel	Indoor
Interferer Number	0
Rake Finger	4
Number of Frame	1

If the user chooses to run the downlink simulator, then downlink button needs to be pressed after typing in the command wcdma at the Matlab prompt. As far as the parameters are concerned, they have the similar significance as those in the uplink simulator. The only change in the default parameters is there are three fingers at the rake receiver unlike four fingers at the uplink.

After the simulation is complete, the simulator provides the user with the options of observing the results in either tabular or graphical form. For example, the user can select the' BER Plot ' button to see the BER performance of the receiver or he can select the ' Display BER ' button to see a table of BER vs E_b/N_0. The final menu for the uplink is shown next.

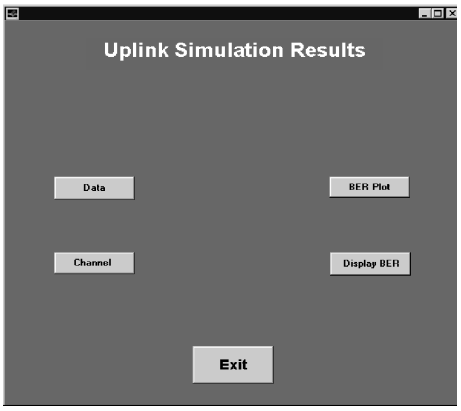

Figure 3.21: Final Menu for the Uplink Simulator

3.5 Code Structure of the Simulator

This section contains a detailed description of the program files used in the simulator. Most of the code of the simulator was written in MATLAB. The following flowcharts illustrate the file structure of the uplink and downlink simulators:

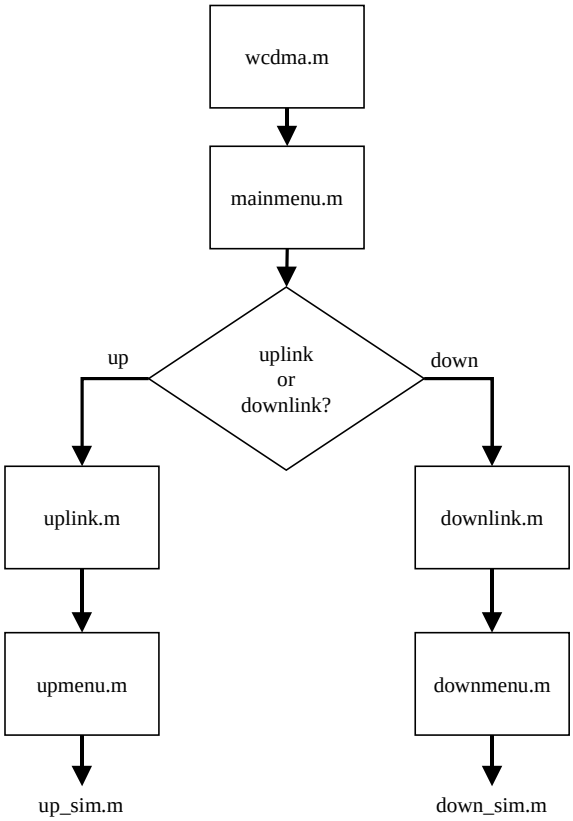

Figure 3.22a: Simulator Code Structure

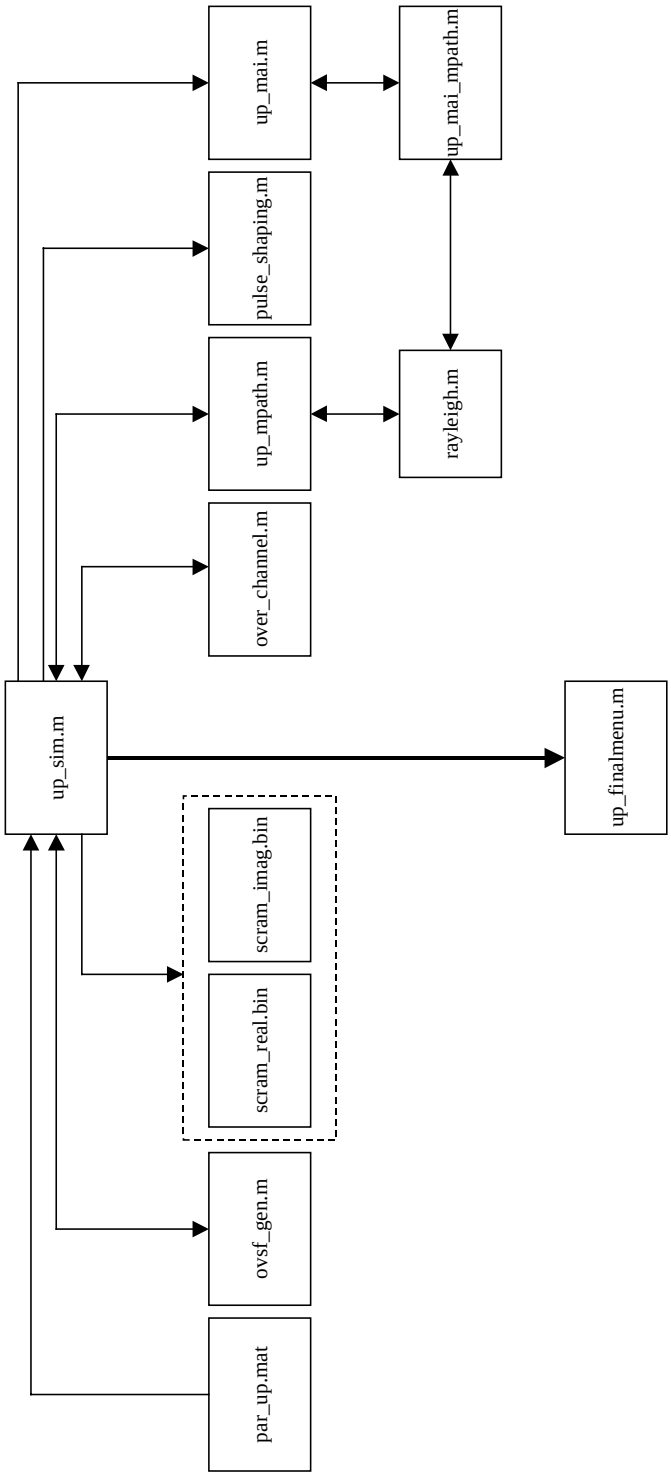

Figure 3.22b: Simulator Code Structure Continued (Uplink Simulator)

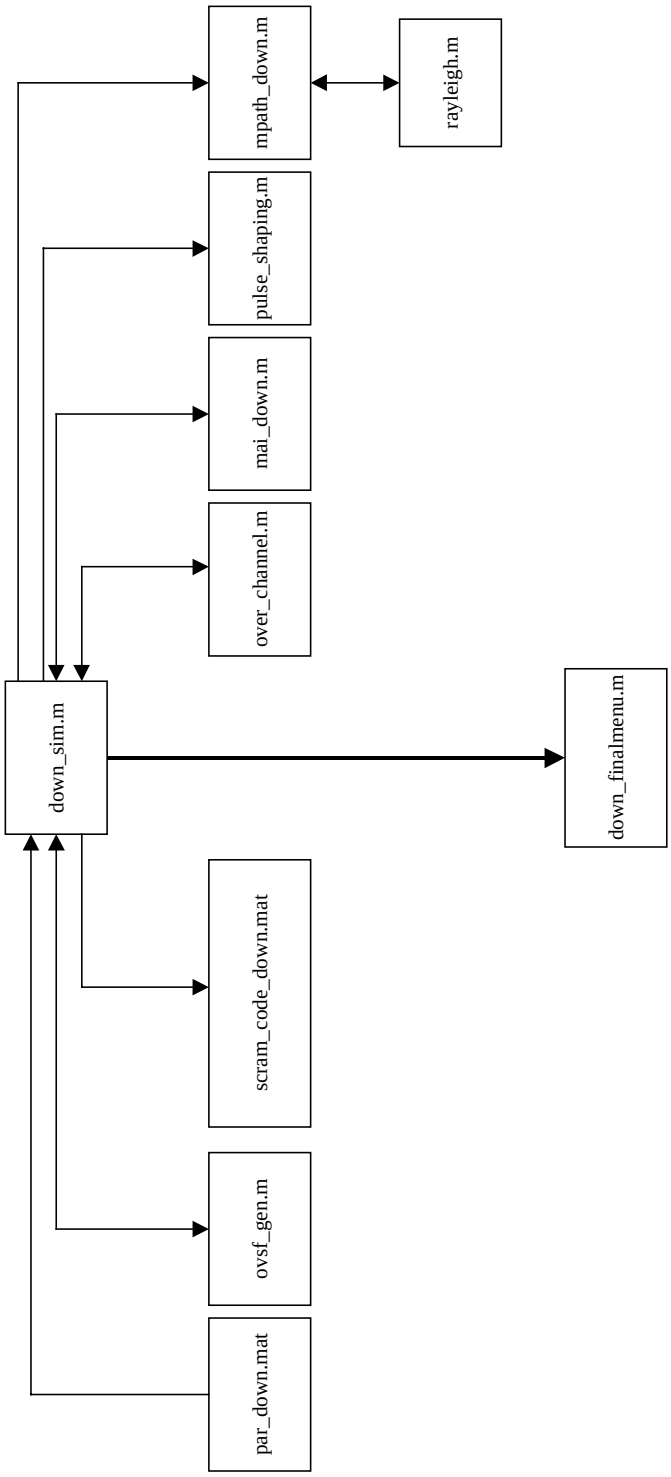

Figure 3.22c: Simulator Code Structure Continued (Downlink Simulator)

3.6 Code Optimization

The simulator was implemented in MATLAB to take advantage of the built-in functions that perform various signal processing application like filtering and Fast Fourier Transformation (FFT) and the superior array handling capability. To make the simulator run within a reasonable simulation time, we had to optimize the MATLAB code. We generated the complex scrambling codes separately and stored them in binary data files. During the simulation run, the simulator reads the desired scrambling codes form these data files. This was necessary since the generation of long scrambling code takes long time and it would not be practical to generate the scrambling codes during running the simulator.

Figure 3.23 shows the MATLAB profile of the uplink simulator. The simulator is run for Vehicular A Outdoor Channel with one interfering user. The Rayleigh waveform is generated at the chip rate. As we notice the simulator spends significant amount of time in lines 184 and 173. They correspond to the functions implementing MAI and time varying channel respectively. The generation of Rayleigh waveform takes up most of the simulation time in both the functions. However generating Rayleigh waveform at symbol rate rather than at chip rate can significantly reduce the simulation time. Another way to reduce the simulation time is to demodulate the signals from the all the interfering users and count their errors towards the BER calculation. However this will increase the complexity of the receiver implementation and we will not have the option of assigning different spreading factors for different users.

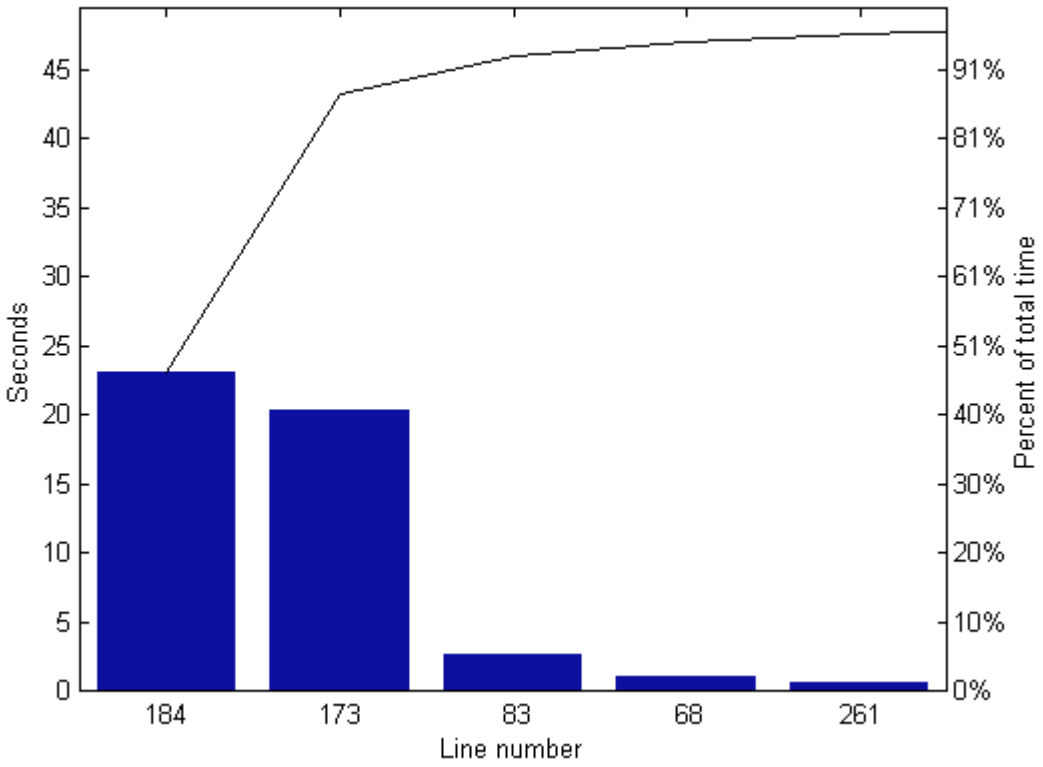

Figure 3.23: Profile of the Uplink Simulator

Chapter 4

Simulation Results

This chapter presents the simulation results for the WCDMA system at different channel conditions. Simulation results include BER/Frame Error Rate (FER) vs E_b/N_0 and BER vs Number of interferers. Improvement in BER due to error correction coding scheme is shown for a 9.6 kbps uplink service.

4.1 Uplink Simulation Results

The following figures show the BER vs E_b/N_0 curves for different number of users. The spreading factor at the data channel is 32. The channels are Indoor channel and Vehicular A Outdoor Channel. The simulation resolution is 5 samples per chip. We assume that the received signals from all the users at the base station have equal power, i.e. we have perfect power control.

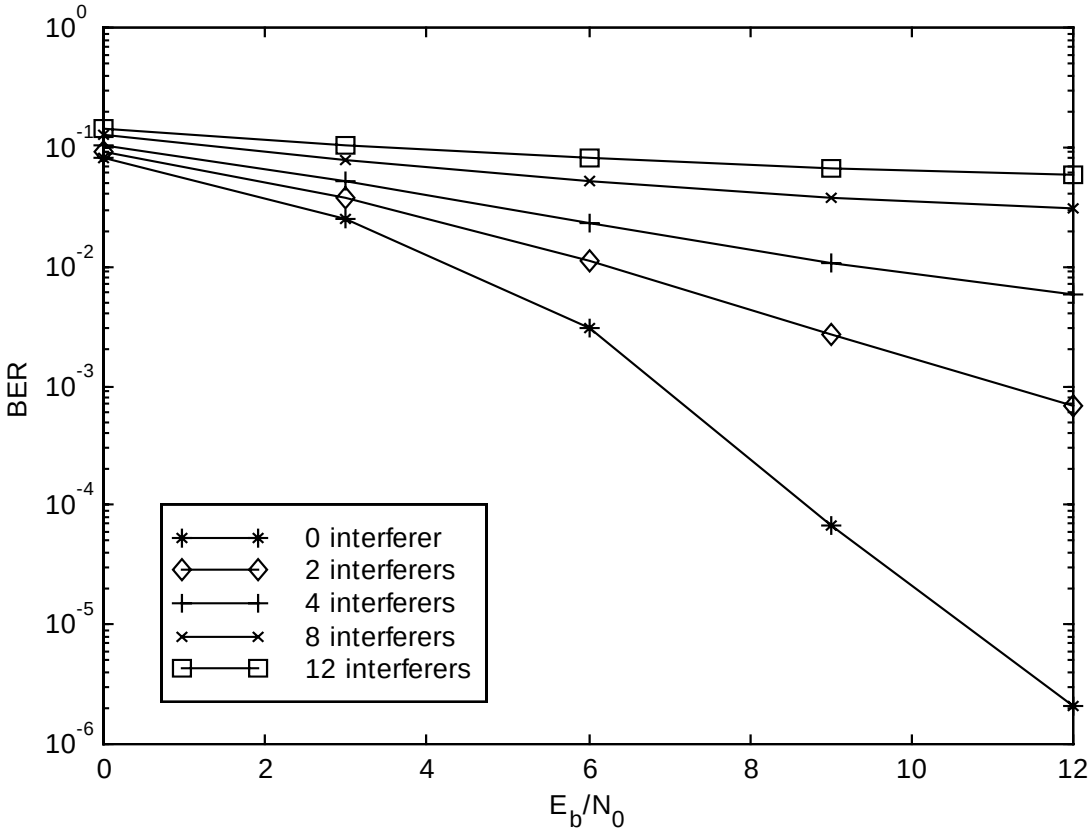

Figure 4.1: BER vs E_b/N_0 at the WCDMA Uplink for Indoor Channel.

(The Spreading Factor of the User is 32.The Number of Interferers Vary from 0 to 12)

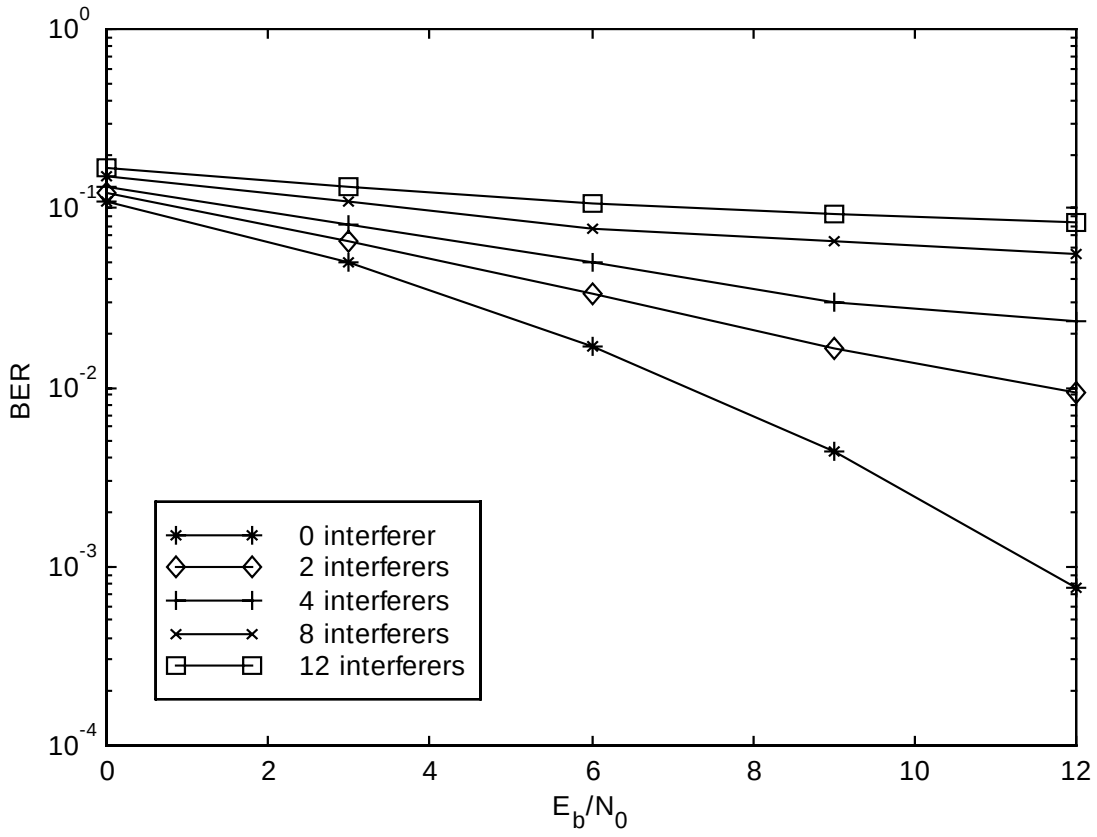

Figure 4.2: BER vs E_b/N_0 at the WCDMA Uplink for Vehicular A Outdoor Channel. (The Spreading Factor of the User is 32. The Number of Interferers Vary from 0 to 12)

We can see from Figure 4.1 and 4.2 that the system becomes interference limited as the number of interferer increases. This is expected for any communications system employing CDMA as the multiple access technique.

Figure 4.3 and 4.4 show the BER vs Number of interfering users. The SNR is fixed at 12 dB. As before, the simulation resolution is 5 samples per chip for both the channels.

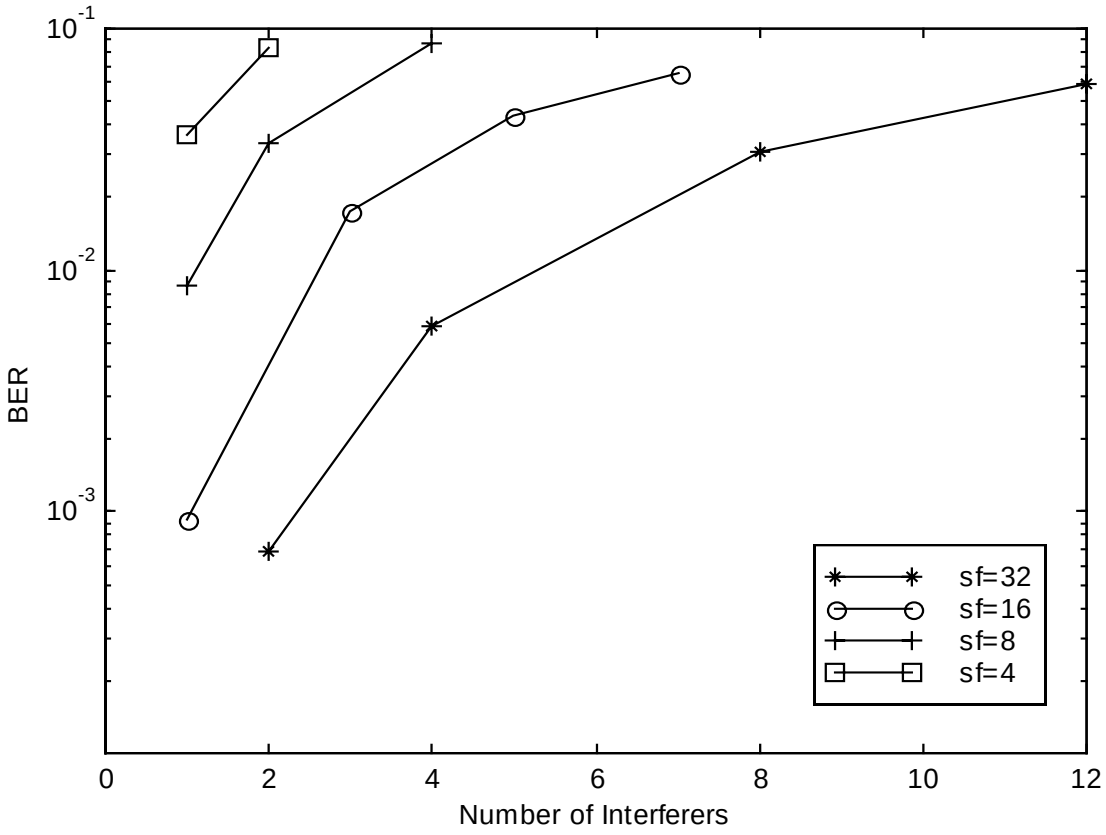

Figure 4.3: BER vs Interferers at the WCDMA Uplink for Indoor Channel. (E_b/N_0 is 12 dB)

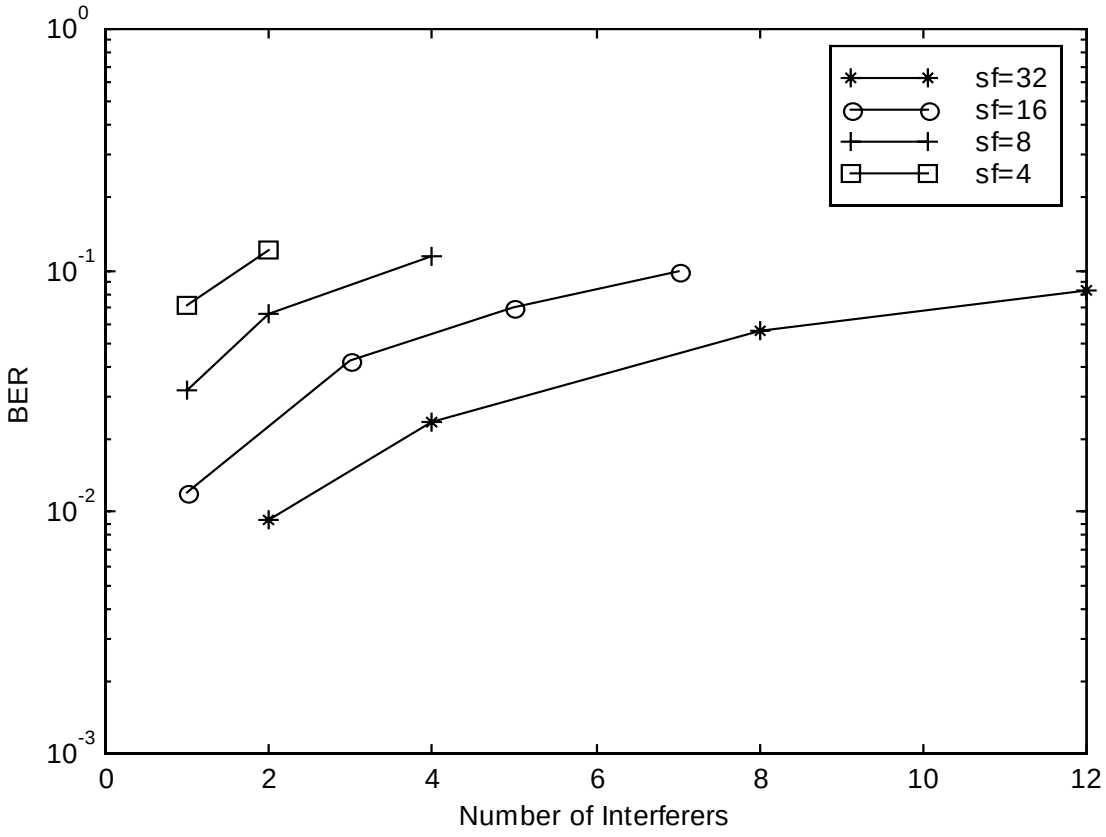

Figure 4.4: BER vs Interferers at the WCDMA Uplink for Vehicular A Outdoor Channel.(E_b/N_0 is 12 dB)

We can observe from the figures that as the system load reaches 50%, the BER approaches to 10% which obviously is unacceptable. However with error correction coding and antenna diversity schemes, the BER can be pushed back to an acceptable limit.

4.2 Downlink Simulation Results

BER performance at the downlink is presented in this section. The following figures illustrates the BER vs E_b/N_0 curves at the downlink for different number of interfering users. The simulation resolution is 5 samples per chip. BER for both Indoor channel and Vehicular A Outdoor channel is shown. The spreading factor is 32. We assume that the signals for all the users are transmitted at equal power.

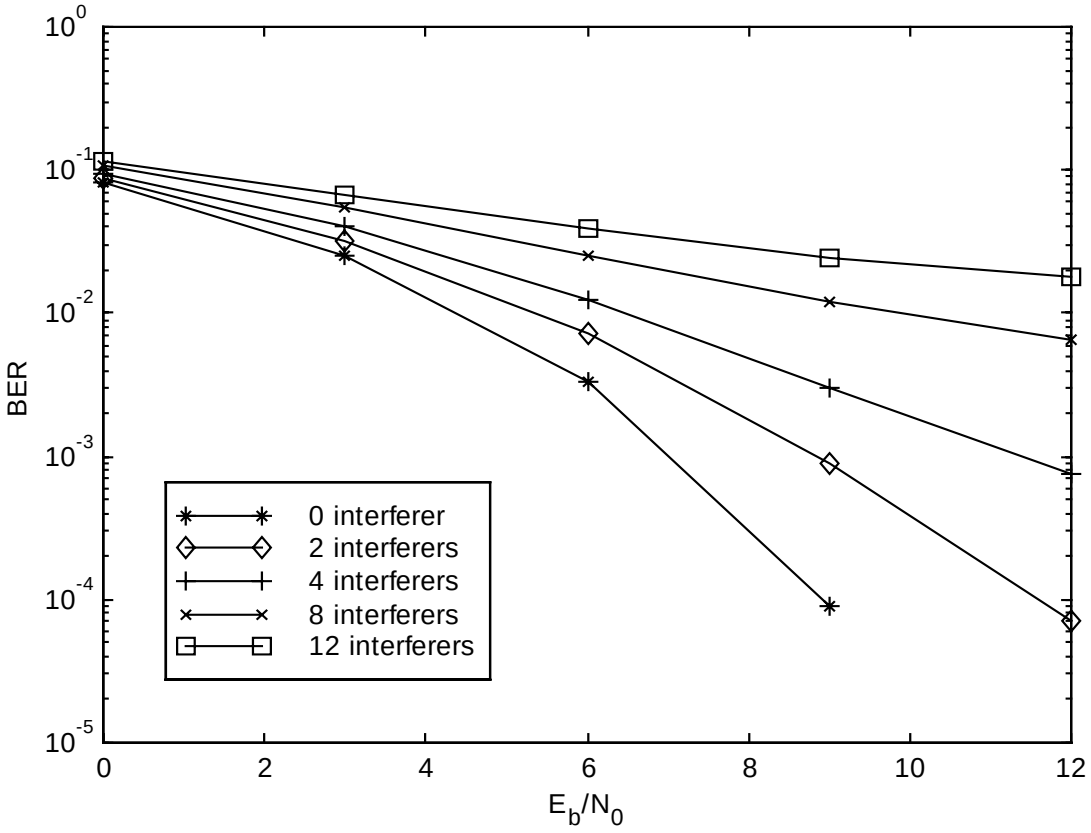

Figure 4.5: BER vs E_b/N_0 at the WCDMA Downlink for Indoor Channel.
(The Spreading Factor of the User is 32. The Number of Interferers Vary from 0 to 12)

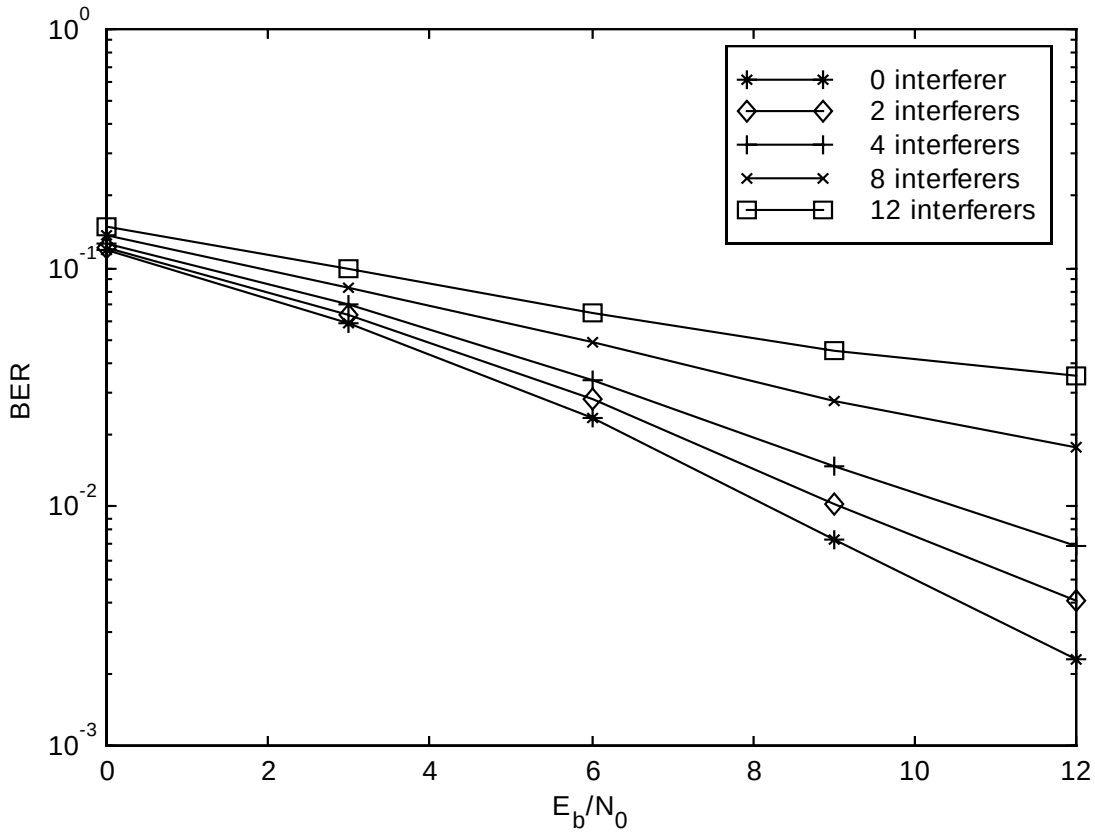

Figure 4.6: BER vs E_b/N_0 at the WCDMA Downlink for Vehicular A Outdoor Channel. (The Spreading Factor of the User is 32. The Number of Interferers Vary from 0 to 12)

As in the uplink, the system is interference limited at the downlink for higher number of interfering users. However, since the users are synchronized, the orthogonality among users is better at the downlink.

Figure 4.7 and 4.8 show the BER vs Number of interfering users. The SNR is fixed at 12 dB. As before, the simulation resolution is 5 samples per chip for both the channels.

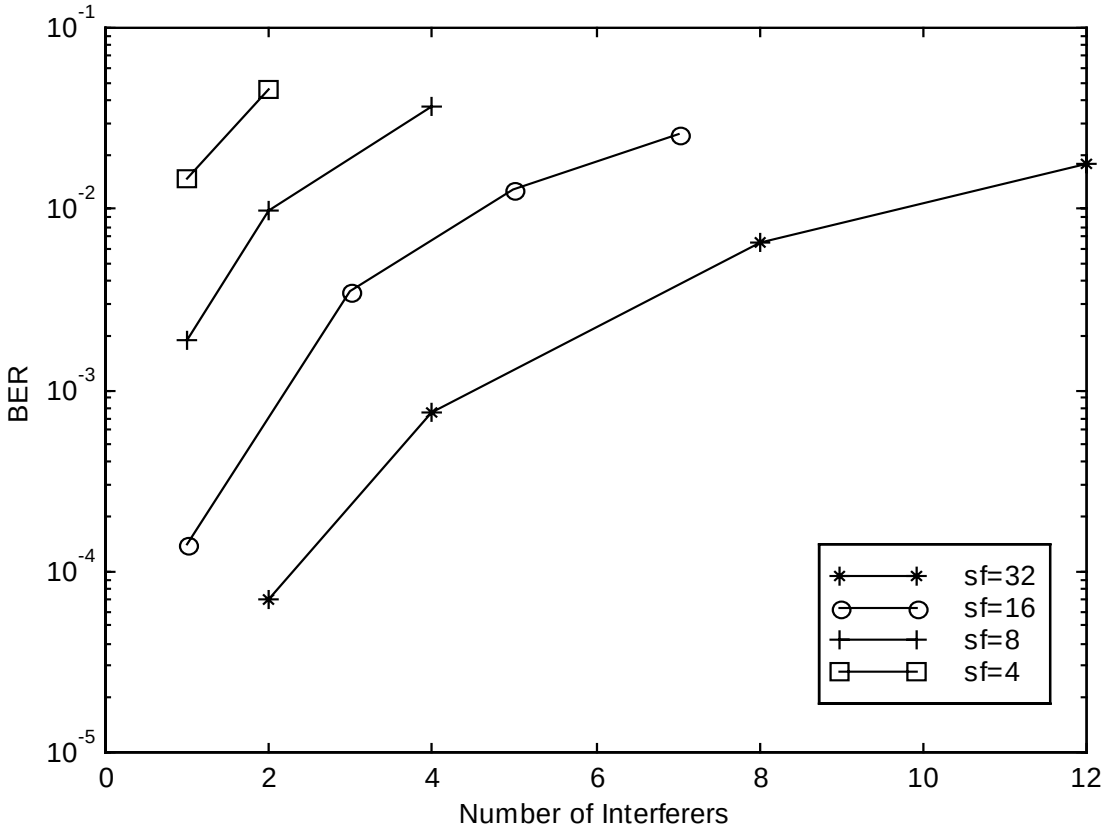

Figure 4.7: BER vs Interferers at the WCDMA Downlink for Indoor Channel. (E_b/N_0 is 12 dB)

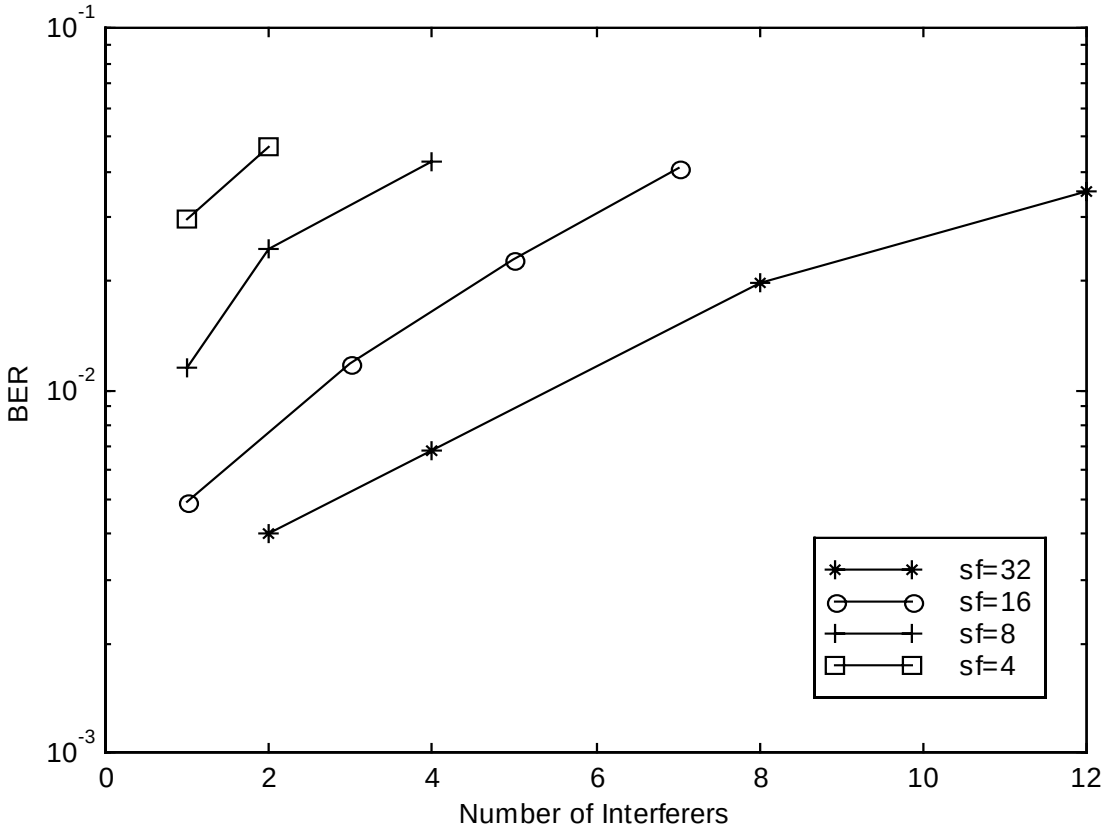

Figure 4.8: BER vs Interferers at the WCDMA Downlink for Vehicular A Outdoor Channel.(E_b/N_0 is 12 dB)

4.3 Coded System

A test case of error correction coding was implemented for an uplink voice application that has a data rate of 9.6 kbps. A rate 1/3 constraint length 9 convolutional coding was employed at the transmitter. A Viterbi soft decision decoder was used at the receiver. We did not implement any error detection scheme or interleaving with that. The following figure shows the encoder used at the transmitter:

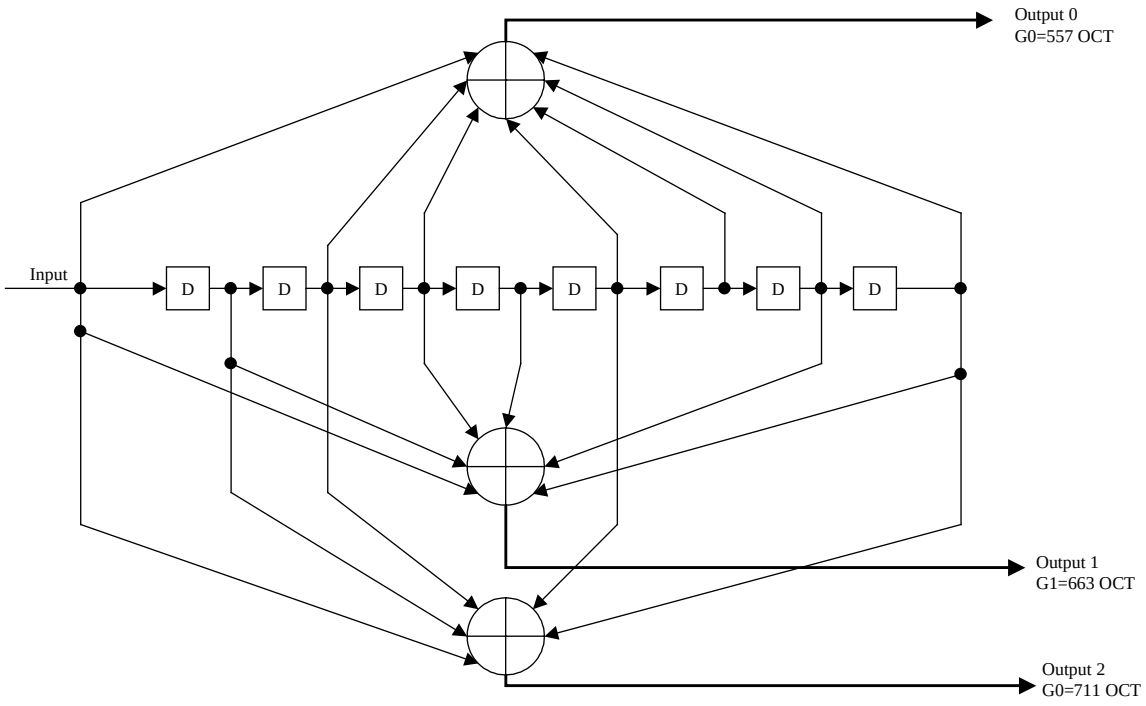

Figure 4.9: Convolutional Coding Scheme

The data rate out of the vocoder is 8 kbps for a voice service of 9.6 kbps. So there are 80 data bits in a frame of 10 ms. 16 more bits are added with each frame as Cyclic Redundancy Check (CRC). So we have 96 bits for each 10 ms frame resulting in an uncoded data rate of 9.6 kbps. The number of tail bits to be added is decided as one less than the

constraint length. So for a constraint length 9 convolutional coding 8 tail bits are added. So if the code rate is 1/3, Code frame size $= (96+8)\times 3 = 312$ bits

The closest frame size available is 300 bits. So 12 bits are punctured at each frame to perform rate matching. A frame size of 300 bits corresponds to a spreading factor of 128.

The following figures show the Frame Error Rate (FER) curves along with BER curves for the coded system:

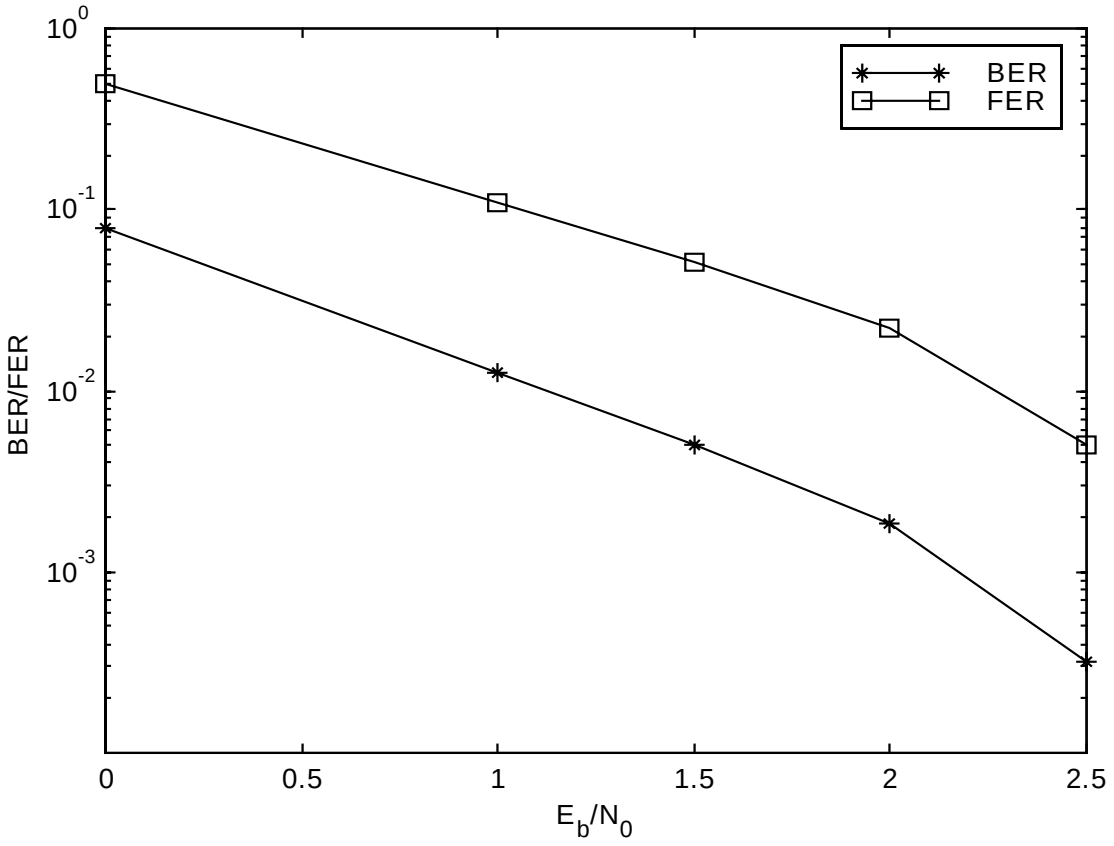

Figure 4.10: Uplink Performance for the 9.6 kbps Voice Service in Indoor Channel. (Constraint Length 9, Rate 1/3 Convolutional Coding is Used.)

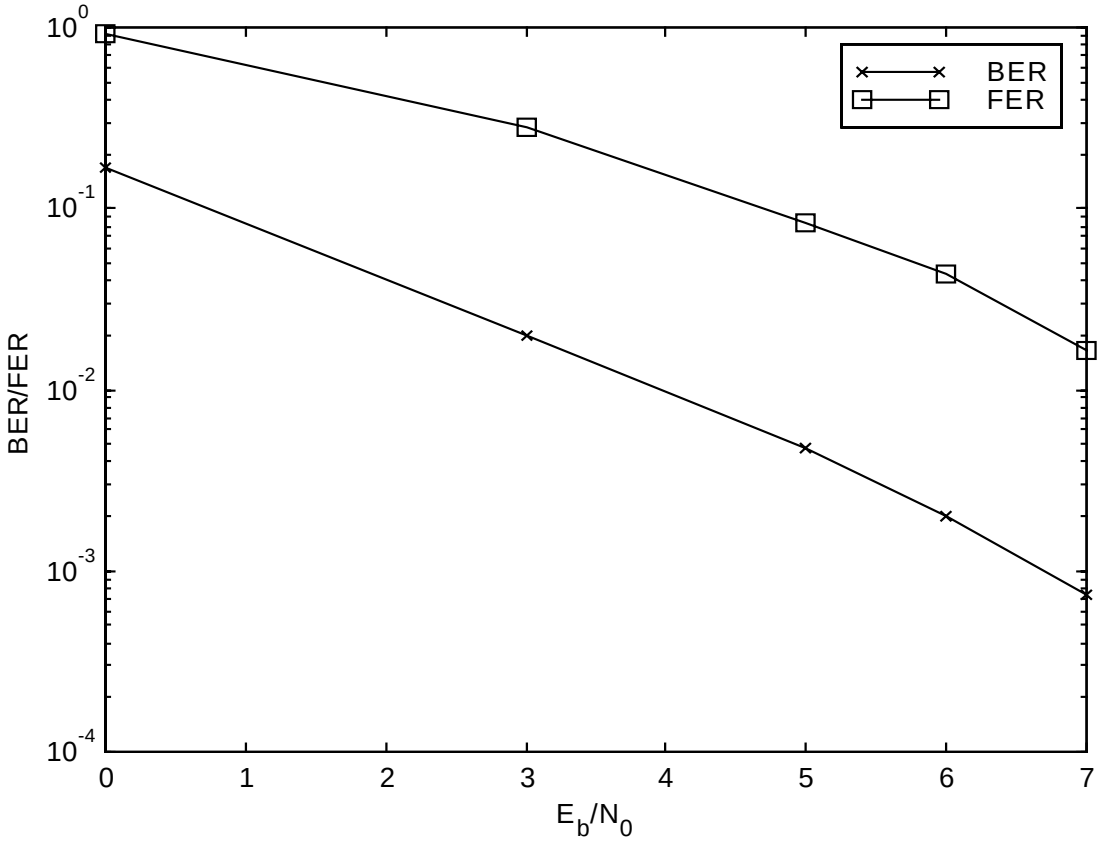

Figure 4.11: Uplink Performance for the 9.6 kbps Voice Service in Vehicular A Outdoor Channel. (Constraint Length 9, Rate 1/3 Convolutional Coding is Used.)

As we can see we get improvement in the BER performance of the system because of the coding gain. The following table compares the E_b/N_0 values required to achieve BER of 10^{-3} for both the coded and the uncoded system at Indoor and Vehicular A Outdoor environment.

Table 4.1: Performance Improvement due to Coding (Target BER=10^{-3})

Channel	Required SNR for Uncoded System	Required SNR for Coded System
Indoor	6.8 dB	2.1 dB
Vehicular A	11.5 dB	6.75

It is evident that we get a coding gain of approximately 4.7 dB for the uplink service of 9.6 kbps.

4.4 Summary of Results

- Orthogonality among channels is preserved better at the downlink.
- The system is interference limited at both the links for higher number of users.
- As the system load approaches 50%, the performance for the uncoded system becomes unacceptable.
- Convolutional coding can provide with a gain of 4.7 dB for 9.6 kbps voice service at the uplink.

Chapter 5

Conclusion and Future Work

We implemented a signal simulator according to the physical layer specification of the IMT-2000 WCDMA system. The data is transmitted in a frame by frame basis through a time varying channel. The transmitted signal is corrupted by multiple access interference. The signal is further corrupted by AWGN at the front end of the receiver. Simple rake diversity combining is employed at the receiver.

We investigated the bit error rate at both uplink and downlink for two different time varying channels. As expected the system is interference limited for higher number of users. We observed that without any channel coding schemes and antenna diversity techniques, the BER approaches to 10% as the system load goes beyond 50%. This is not an acceptable performance. However the BER can be pushed back to an acceptable limit with channel coding and antenna diversity techniques.

The developed simulator can be an invaluable tool to investigate the performance of a WCDMA under various conditions. As for example the simulator can be used to investigate antenna diversity schemes at the receiver. The simulator is very flexible and one can very easily make the necessary modification to incorporate complex statistical

channel model based on measurement and investigate the WCDMA performance under practical mobile channel condition. We have shown that it is very simple to employ the simulator to observe the performance of error correction coding. We implemented a convolutional coding scheme for an uplink voice application of 9.6 kbps. It was observed that channel coding could significantly lower the required SNR for a particular BER.

5.1 Future Work

The simulator employs a simple rake receiver to exploit the gain arising from temporal diversity. Spatial property of the multipath environment can be another source of diversity. Adaptive antennas are used at the receiver to take the advantage of this diversity gain. The simulator can be used to investigate the diversity gain of different adaptive algorithms. Space-Time rake receivers [21], [22] or 2-D rake receivers [23] have been proposed to combine the temporal and spatial diversity at the receiver. Transmit diversity techniques [13], [14] at the downlink are gaining rapid popularity since they do not incur additional hardware complexity at the mobile station. We are investigating various transmit diversity schemes and different 2- D rake receivers for the WCDMA system. The simulator was modified so that a large number of frames are transmitted rather than transmitting one frame at a time.

Turbo coding has been specified for applications that require very low bit error rate. Turbo coding schemes can be incorporated to the simulator in the same way we employed convolutional coding.

The simulator can be further improved by using statistical channel models based on measured data. The improvement in system performance by using multi user detection and interference cancellation can also be investigated.

Bibliography

[1] Malcom W. Oliphant, " The Mobile Phone Meets the Internet," *IEEE Spectrum*, pp. 20-28, August 1999.

[2] Tero Ojanpera and Ramjee Prasad, "An Overview of Air Interface Multiple Access for IMT-2000/UMTS," *IEEE Communications Magazine*, vol. 36, pp. 88-95, September 1998.

[3] Erik Dahlman, Bjorn Gudmundson, Matts Nilsson, and Johan Skold, " UMTS/IMT-2000 Based on Wideband CDMA," *IEEE Communications Magazine*, vol. 36, pp. 70-80, September 1998.

[4] Erik Dahlman, Per Beming, Jens Knutsson, Fredrik Ovesjo, Magnus Persson, and Christiaan Roobol, " WCDMA- The Radio Interface for Future Mobile Multimedia Communications," *IEEE Transactions on Vehicular Technology*, vol. 47, No. 4, pp. 1105-1118, November 1998.

[5] Third Generation Partnership Project Technical Specification Group Radio Access Network Working Group 1," Spreading and Modulation," TS 25.213 V2.1.2 (1999-4).

[6] Third Generation Partnership Project Technical Specification Group Radio Access Network Working Group 1, " Physical Channels and Mapping of Transport Channels onto Physical Channels (FDD)," TS 25.211 V2.2.1 (1999-08).

[7] Kevin Laird, Nick Whinnet, and Soodesh Buljore, " A Peak-To-Average Power Reduction Method for Third Generation CDMA Reverse Links," in Proc., IEEE Vehicular Technology Conference, 1999.

[8] Esmael H. Dinan and Bijan Jabbari, "Spreading Codes for Direct Sequence CDMA and Wideband CDMA Cellular Networks," *IEEE Communications Magazine*, vol. 36, pp. 48-54, September 1998.

[9] T.S. Rappaport, *Wireless Communications: Principles and Practice*. Upper Saddle River, NJ: Prentice Hall PTR, 1996.

[10] Third Generation Partnership Project Technical Specification Group Radio Access Network Working Group 1, " Multiplexing and Channel Coding (FDD)," TS 25.212 V2.0.1 (1999-08).

[11] Alpha Concept Group, "Wideband Direct Sequence CDMA (WCDMA) Evaluation Document (3.0)," Tdoc SMG 905/97, December 15-19, 1997, Madrid, Spain.

[12] J. C. Liberti and T.S. Rappaport, *Analysis of CDMA Cellular Radio Systems Employing Adaptive Antennas*. PhD dissertation, Virginia Tech, Blacksburg, VA, September 1995.

[13] S.M. Alamouti, "A Simple Transmit Diversity Technique for Wireless Communications," IEEE Journal on Selected Areas in Communications, vol. 16, pp. 1451-1458, October 1998.

[14] Texas Instruments, "Space Time Block Coded Transmit Antenna Diversity for WCDMA," ETSI SMG-2 UMTS-L1, TDOC 662/98.

[15] Third Generation Partnership Project Technical Specification Group Radio Access Network Working Group 1, " Physical Layer Procedures (FDD)," TS 25.214 V1.1.2 (1999-08).

[16] Commission of the European Communities, " *Digital Land Mobile Radio Communications: COST-207 Final Report*," chapter 2, 1988.

[17] W.C. Jakes, *Microwave Mobile Communications*. John Wiley and Sons, 1974.

[18] R. Price and P.E. Green," A communications technique for multipath channels," Proceedings of the IRE, vol. 2, pp. 555-570, March 1958.

[19] J. G. Proakis, *Digital Communications*. New York, NY: McGraw-Hill Inc., third ed., 1995.

[20] Roger L. Peterson, Rodger E. Ziemer, and David E. Broth, *Introduction to Spread Spectrum Communications*. Englewood Cliffs, NJ: Prentice Hall, 1995.

[21] Javier Ramos, Michael D. Zoltowski, and Hui Liu, "A Low-Complexity Space-Time Receiver for DS-CDMA Communications," *IEEE Signal Processing Letters*, vol. 4, No. 9, pp. 262-265, September 1997.

[22] B. Xu, T.B. Vu, and H. Mehrpour, "A Space-Time Rake Receiver for Asynchronous DS-CDMA System Based on Smart Antenna," in *Proc., IEEE Vehicular Technology Conference*, 1999.

[23] Babak h. Khalaj, Arogyaswami Paulraj, and Thomas Kailath, "2 D Rake Receivers for CDMA Cellular Systems," in *Proc., IEEE Globecom Conference*, pp. 400-404, 1994.

Vita

Fakhrul Alam was born in Dhaka, Bangladesh on April 18, 1972. He received his B.Sc. Degree in Electrical and Electronic Engineering from Bangladesh University of Engineering and Technology (BUET). He worked as a lecturer in the EEE Department of his alma mater for a year. He started in the M.S. program at Virginia Tech from the fall of 97 and joined MPRG in the fall of 98. His research interests include Adaptive Receivers for Narrow and Wide Band Modulation Schemes, Space-Time Coding and Wideband CDMA Systems. He will continue as a Ph.D. student with Dr. Brian D. Woerner from spring of 2000.